Journal of Rheology

Nonlinear shear rheology of single and double dynamics metal-ligand networks

Christina Pyromali[1,2*], Yanzhao Li[3], Flanco Zhuge[3], Charles-André Fustin[3], Evelyne van Ruymbeke[3] and Dimitris Vlassopoulos[1,2]

[1]Institute of Electronic Structure & Laser, FORTH, Heraklion 71110, Crete, Greece

[2] Department of Materials Science and Technology, University of Crete, Heraklion 71003, Crete, Greece

[3]Bio-and Soft Matter, Institute of Condensed Matter and Nanosciences, Université Catholique de Louvain, Croix du Sud 1, B-1348 Louvain-la-Neuve B-1348, Belgium

ABSTRACT

We present a systematic experimental study of the shear rheology of metallo-supramolecular assemblies based on entangled telechelic star polymers comprising one (single dynamic network) or two (double dynamics network) types of physical bonds, with the aim to unravel the role of concentration and strength of these bonds on the nonlinear response. Model dynamic networks functionalized with terpyridine ligands were formed by adding different metal ions with increasing bonding strength, zinc, copper and cobalt. The dynamics are driven by entanglement/disentanglement processes and ligand exchange mechanism. Steady-state viscosities of single and double dynamics networks collapse onto a universal curve over a wide range of Weissenberg numbers based on terminal time (up to about 300 for single and 1000 for double) exhibiting weaker shear thinning (with exponent of -0.76) compared to entangled neutral polymers. Double dynamics networks consisting of two different metal ions (with different lifetimes) exhibit stronger mechanical coherence (rate-dependent fractional viscosity overshoot) and accumulate larger strain at steady-state flow compared to single ion counterparts. The shear stress growth function signals exhibit weak, albeit unambiguous shear strain hardening which becomes more pronounced for stronger associations. They also exhibit double overshoot which

reflects the interplay of association strength and chain deformation. Increasing the strength of associations leads to failure of the Cox-Merz rule, which is more severe for single dynamic networks. The markedly different behavior of double dynamics networks is attributed to the fact that at sufficiently high ion content the weaker bond acts as sacrificial component which provides local energy dissipation and enhance the overall deformability. This bears analogies with their linear viscoelastic response which has revealed that the arm disentanglement (delayed due to the reversible bonds) effectively interpolates between the two single dynamic network components, depending on composition. Our results suggest ways to tailor the mechanical properties of this class of materials by judicious choice of the ions type and content.

I. INTRODUCTION

Associating and supramolecular polymers have been the subject of extensive investigations for over three decades because of their versatility and reversible directional interactions that dictate their macroscopic properties [1–3]. Indeed, non-covalent interactions such as hydrogen bonding, metal-ligand coordination, π-π stacking and host-guest interaction can be triggered by external environment [4] or shear stress and their adaptability gives rise to intriguing features including tunability, self-healing and mechanical reinforcement [5–6]. Reversibility of these types of macromolecules is related to self-healing and represents a major asset for novel applications in tissue remodeling [7], light-induced adhesives [8], self-healing coatings [9] and stretchable electronics [10]. In this work we focus on associating telechelic polymeric networks. To obtain associating polymers with desired properties it is imperative to fundamentally understand the relationship between structure and dynamics. The latter are driven by chain relaxation (which may reflect entanglement/disentanglement) processes and association dynamics [3]. Consequently, the interplay of these two modes (chain and bonding) in the rheological response should be unraveled and understood. Theoretical and experimental studies with associating polymers have focused primarily on the linear viscoelastic properties. The sticky-Rouse model is extensively used [11–12] for the description of dynamics of reversible networks considering chain movement via stickers breakage and reconstruction. Topological constrains slow-down the stress relaxation process because of the presence of entanglements. The sticky reptation model describes the molecular motion of entangled chains that is delayed by the association/dissociation events, so the

stress relaxation function is characterized by two plateau regimes: one at shorter times, due to sticker associations, and another with lower value at longer times, due to chain entanglements [13–14]. Molecular dynamics simulations of the dynamics of unentangled telechelic polymer solutions forming clusters, have revealed a two-step stress relaxation mechanism. It comprises a stress decay due to the end-groups rearrangement within the cluster, and a diffusive hopping of the end-group to another cluster, which depends on the bond lifetime [15]. Along the same lines, entangled telechelic stars also exhibit complex relaxation characterized by both structural (due to bonds) and topological (entanglements) responses [16]; in the case of very strong (sulfur-sulfur) associations, experiments and coarse-grained simulations confirmed the absence of terminal relaxation and showed that the stress relaxation reflected the relative importance of intra- and inter-molecular bonding [17]. Recent investigations of ionomers show how one may use linear and nonlinear rheology to extract the magnitude of sticker lifetime, the association energy and the distribution of relaxation times, as well as to tailor flow and mechanical properties of these materials [11, 18–21]. Zhuge and co-workers used the modified tube-based Time Marching Algorithm (TMA) model in order to decode the linear viscoelastic response of weakly entangled telechelic metallo-supramolecular stars in the melt state. In this model, the stress relaxation modulus G(t) accounts for chain and sticker relaxation processes, in similar way to sticky Rouse or sticky reptation [22]. The model also incorporates the delayed fluctuations due to the sticker lifetime and the association/dissociation dynamics (in particular, the time during which a sticker is free, τ_{free}) as discussed in Refs. [23] and [24].

Concerning the nonlinear shear properties of associating and supramolecular polymers, the failure of the empirical Cox-Merz rule has been widely reported in the literature [25–30]. Many studies reveal that the steady shear viscosity exceeds the complex viscosity. Shear thickening has been observed at intermediate shear rates, with the association strength playing a major role in the phenomenon [31]. A mean-field approach indicated that shear thickening in ionomer solutions is related to shear-induced modification of the coupling between intramolecular to intermolecular associations [32]. Suzuki and co-workers suggested that thickening was primarily due to fact that recombination of associations at a given shear rate outbalances their destruction [27, 33]. Shear-thinning behavior has always been observed at very fast flows, following thickening or directly the Newtonian plateau. Caram et al. [26] studied the rheology of hydrophobic associative polymers (HASE) and rationalized the failure of Cox-Merz rule using a multi-mode model with a kinetic

balance between the prevailing destruction of long-range associations and the formation of short-range associations. During startup of steady shear flow, associating polymers were reported to exhibit shear strain hardening of the shear stress growth function, a phenomenon attributed to the finite extensible nonlinear elasticity (FENE) of these materials (promoted by the associations) with the support of simulations and transient network theory [33–39]. The peak of shear stress growth function, observed at certain time (or strain) for a given imposed shear rate, is often called (static) yield stress or maximum stress, and the respective strain is the yield strain or strain at maximum stress. In several studies, the yield point (stress and strain) has been reported to depend on shear rate [37–38, 40–43]. This reflects the coupling of dissociation rate and chain tension [37]. The strength of associations is important in this respect, and its role has not been explored systematically with the same polymeric melt and different crosslinking density and type of sticker.

The properties of single lifetime transient networks can be reinforced either by adding long non-associating polymers [44] or by mixing two different types of interactions [45]. In general, double networks (DNs) having one constituent with chemical bonds and another with physical bonds exhibit enhanced mechanical properties such as toughness and extensibility [46–50]. The mechanism behind these properties is based on the combination of two interpenetrating networks with one transient component that acts as a sacrificial bond, and a second permanent network that gives coherence and stiffness [51–53]. The double dynamics networks (DDNs), which are made of two reversible networks, emerged from the realization that the covalent crosslinks of a permanent chemical network become irreversibly damaged under strong mechanical deformation, losing the advantage of improved mechanical properties. To overcome this limitation, covalent bonds were replaced by reversible bonds, forming the so-called double dynamics networks [46, 49]. The consequences of this approach in improving the mechanical properties of materials have been explored particularly in the context of self-healing of hydrogels [54–55]. However, the rheological behavior of DDNs in the melt state has not been investigated so far.

In this work we present as systematic experimental investigation of the nonlinear shear rheological properties of single and double dynamics networks based on entangled telechelic star polymers associating by means of metal-ligand interactions with different strength (metals). The particular double dynamics networks used comprise the same polymer (here a poly(n-butyl acrylate) star with 4 arms) forming metal-ligand associations with two different metals, reflecting different

strengths. They are simpler compared to those typically used in applications, which involve two chemically different interpenetrating networks [7, 47-53]. Such well-characterized materials are used to address fundamental questions concerning their rheology. In particular, we discuss here the validity of the Cox-Merz rule and the features of the shear stress growth function signal for different metal-ligand interactions and temperatures.

II. EXPERIMENTAL

Materials

Each network consists of a four-arm telechelic poly(n-butyl acrylate), PnBA, star with total number average molar mass of about 250 kg/mol (corresponding to weakly entangled arms with $Z \approx 3.4$ entanglements), polydispersity of 1.2, and end-functionalization with a terpyridine reactive end-group. The latter was synthesized by reversible addition—fragmentation chain-transfer (RAFT) [23, 56] (see Figure 1a). The terpyridine ligands associate with different metal ions, added in the form of salts (zinc chloride, copper chloride and cobalt chloride) at three different stoichiometric amounts (0.5eq. 0.75eq & 1.0eq. per eq. of terpyridine ligand).

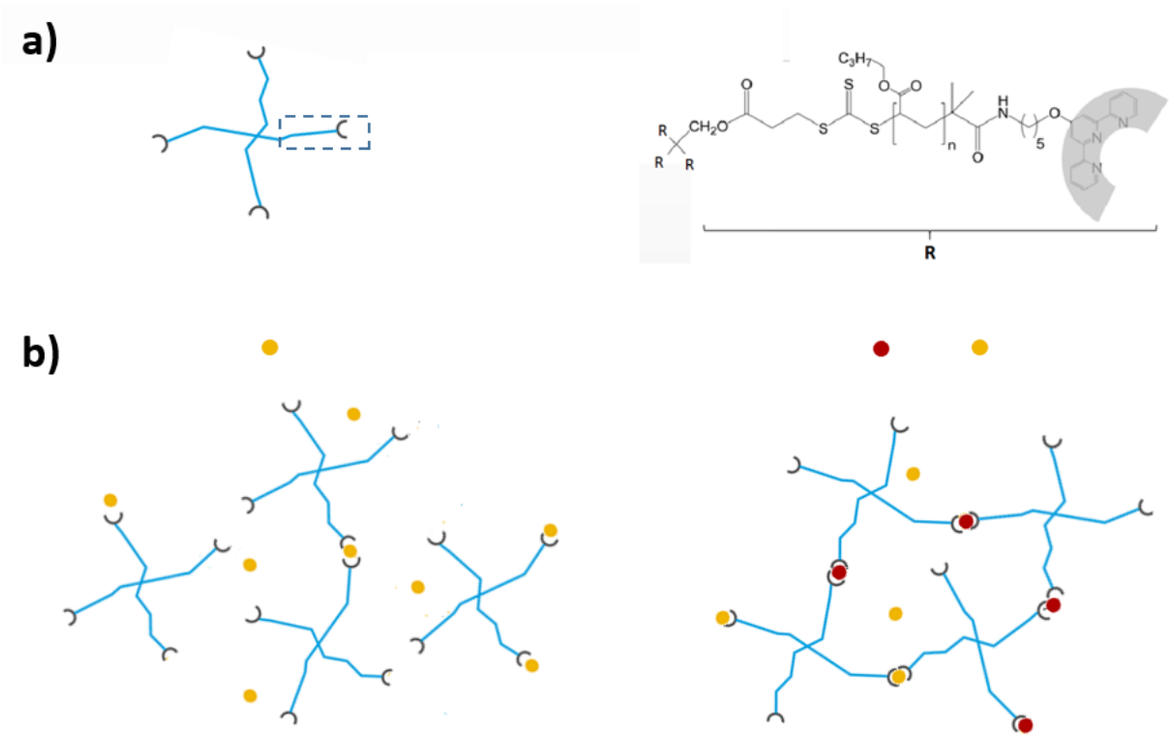

Figure 1. (a) Schematic of the 4-arm telechelic star functionalized with terpyridine ligands. Taken from [22] with modifications. (b) Schematic illustration of transient networks formed by single (left) and double (right) lifetime junctions.

The selected metal ions are suitable for comparison since they have same positive charge, similar size and thermodynamic stability. More importantly, they form bis(terpyridine) complexes at stoichiometric amounts [57]. The relevant kinetics depends on the different binding constants for formation mono-complexes and bis-complexes, influencing the stability of the dynamic network (see Table S1 of the Supplementary Material, SM). As discussed in ref. [22], zinc associations are expected to be labile, copper tends to form more mono-complexes and cobalt forms equally stable and stronger mono-complexes and bis-complexes. While Cu(II) bis-complexes were found to be more stable and longer living in comparison to Zn(II) networks, it was also shown that the stability of bis-complexes was promoted by adding excess of metal ions [23]. Given that the dangling chains of the telechelic stars may relax before being (re)-associated, samples containing an excess of ions (0.75eq. and 1.0eq. of the metal ion per 1.0eq. of terpyridine ligand) were used, compared to the theoretical stoichiometric ratio of 0.5eq. of ions per 1.0eq. of terpyridine ligands. More

specifically, with the help of TMA modeling, the linear dynamics study revealed that the fraction of dangling ends (p_{dang}) decreased significantly with increasing the amount of metal ions [23].

Analysis of the linear viscoelastic data indicated that the star arms extremities, which can change their state from dissociated to associated metal-ligand complexes, act as extra frictional points slowing-down the overall stress relaxation of the star arms [22–23]. Indeed, the relaxation of the latter could be accurately described by considering that, apart from a fraction of dangling ends (p_{dang}) able to relax at short time, the star arms can only relax at the average time during which their corresponding sticker was free to move move; this average time corresponds to a fraction p_{free} of the time t elapsed ($p_{free}t$). As the probability of a sticker to be free strongly depends on the ion type, double dynamics can arise from the friction asymmetry when two single transient networks of different type of metal ions are blended (Figure 1b). The complete list of the samples used in this work is presented in Table 1 and further details about metal ion incorporation protocols and molecular characteristics of the constituents can be found in Refs. [22] and [23].

Table 1. Investigated samples annotation and composition

Sample code	**Description**
Star250k-Reference	Precursor sample without metal ions
Star250k-Zn-0.5eq.	Single dynamic network with 0.5eq. Zn(II)
Star250k-Zn-0.75eq.	Single dynamic network with 0.75eq. Zn(II)
Star250k-Zn-1.0eq.	Single dynamic network with 1.0eq. Zn(II)
Star250k-Cu-0.5eq.	Single dynamic network with 0.5eq. Cu(II)
Star250k-Cu-0.75eq.	Single dynamic network with 0.75eq. Cu(II)
Star250k-Cu-1.0eq.	Single dynamic network with 1.0eq. Cu(II)
Star250k-Cu-1.25eq.	Single dynamic network with 1.25eq. Cu(II)
Star250k-Co-0.5eq.	Single dynamic network with 0.5eq. Co(II)
Star250k-Co-0.75eq.	Single dynamic network with 0.75eq. Co(II)
Star250k-Co-1.0eq.	Single dynamic network with 1.0eq. Co(II)
Star250k-ZnCo-0.5eq.	Double dynamics network with 0.25eq. Zn(II) and 0.25eq.Co(II)
Star250k-ZnCu-0.5 eq.	Double dynamics network with 0.25eq. Zn(II) and 0.25eq.Cu(II)
Star250k-ZnCu-1.0 eq.	Double dynamics network with 0.5eq. Zn(II) and 0.5eq.Cu(II)

Rheometry

We used a strain controlled ARES (2kFRTN1) rheometer (TA Instruments) with nitrogen/air flow convection oven that ensures accurate temperature control (±0.1K). Both linear and nonlinear shear measurements were performed with a home-made stainless steel cone-partitioned plate (CPP) geometry in order to reduce the effect of edge fracture when fast shear rates are imposed on the samples [58–59]. The inner measuring plate diameter was 6mm while the inner diameter of the outer ring was 6.2mm and its outer diameter 15mm. The cone diameter was 25mm, its angle 0.1rad and the truncation 51μm. Different geometries were used in order to test reproducibility and accommodate small amounts of sample (inner plate diameter of 4mm). Technical details concerning the measurements are discussed in references [59–60], and in the results section below. After loading, the sample was annealed for 30 minutes at 130^{o}C to ensure thermal equilibration (confirmed by steady moduli values). Then, the temperature was lowered to the measurement temperature (25, 40 or 60^{o}C). For each temperature change, sample equilibration was ensured by performing a dynamic time sweep (DTS) measurement. The gap was adjusted according to the thermal expansion coefficient of the stainless steel tools. An example of DTS is depicted in Figure S1a of the SM. The linear viscoelastic (LVE) regime was determined by means of dynamic strain sweep (DSS) measurements at a given temperature and frequency. Subsequently, dynamic frequency sweeps (DFS) were performed at a fixed temperature and strain amplitude, well within the linear regime, and a frequency range 10^{2}-10^{-2} rad/s. The results were compared with those of references [23] and [56] in terms of reproducibility. The horizontal and vertical shift factors are those of reference [23] for the same samples.

Step-rate measurements were performed at different shear rates ranging from 0.1 to 100 s^{-1}, corresponding to the regime proceeding terminal response based on the LVE data at the particular temperature. Repeat measurements were performed and so were DFS measurements after each step-rate test in order to ensure the reproducibility and confirm the good condition of the sample, especially following fast flows (see Figure S1b). For each sample, measurements were conducted at least at two temperatures with distinct LVE dynamics and ligand exchange mechanism under shear. Figure 2 depicts the shear stress growth coefficient (η^{+}) as a function of time for a typical

startup measurement of a single dynamic network with 1.0eq. Cu. Initially, η^+ increases linearly, reflecting linear elastic deformation. This can be appreciated by the coincidence of the data with the LVE envelope, i.e., the respective DFS data which have been transformed into shear stress growth coefficient data with the help of the Cox-Merz and Gleissle empirical rules [59]. At higher shear rates we observe an overshoot in η^+, which is attributed to the collective orientation and/or stretching of the chain segments and is followed by flow-induced disentanglement/re-entanglement and/or bond break-up/re-arrangement . The maximum, which we identify as yield point, appears on the (moderately) nonlinear regime and becomes enhanced as the shear rate increases, in the strongly nonlinear regime. Finally, η^+ reaches steady-state (flow).

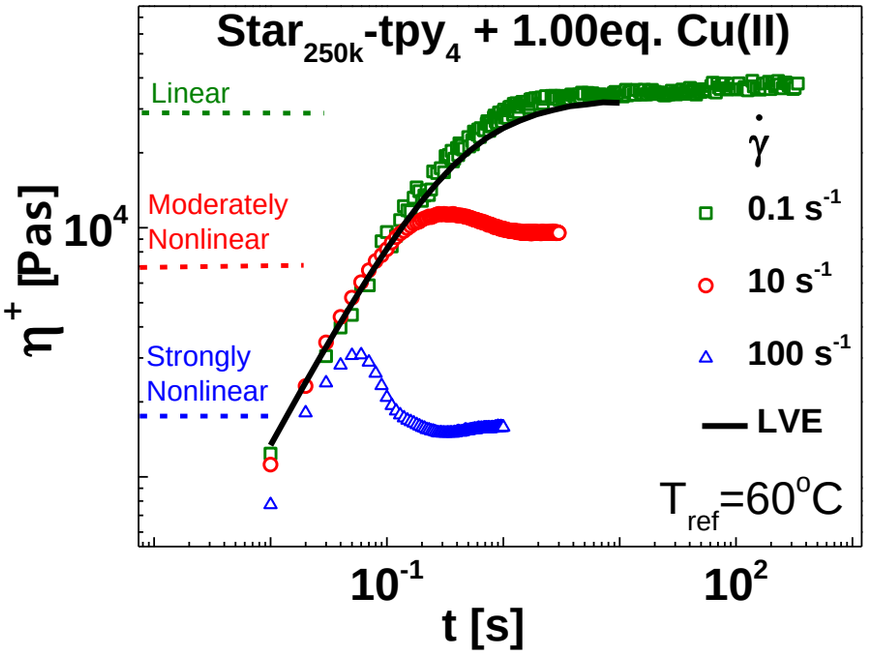

Figure 2. Time-dependent shear stress growth coefficient of Star250k PnBA with 1.00eq. Copper (II) at 60°C.

Differential scanning calorimetry (DSC)

Thermal measurements were performed on Cu(II) single dynamic networks with 0.5eq., 0.75eq. and 1.0eq. of metal ions using DSC 250 (TA Instruments). The samples weighted approximately

5mg and they were placed in Tzero holders. Heat capacity was standardized with sapphire while temperature and enthalpy calibration were conducted with indium standard. Heating /cooling rate was 10 K/min for temperatures ranging from -90 to 120^{o}C. DSC measurements were evaluated at the second heating scan. A typical example is shown in Figure S2 for three samples.

III. RESULTS & DISCUSSION

The combined experimental and modeling study of the linear rheological response unraveled that the dynamics of single and double transient networks depend on both topological constrains and metal-ligand exchange kinetics [22-23]. As already mentioned, their contributions were quantified in the modified TMA by using the fraction of dangling ends (p_{dang}) and the average time duration when a sticker is free (p_{free}). Here, we present start-up shear experiments of the metallo-supramolecular PnBA networks with the aim to understand the nonlinear properties and how to tune them by altering ion type, content and temperature.

A. Single lifetime networks

We start with the nonlinear shear response of single ion components which are the constituents of the DDNs (discussed in section III. B). The available DSC results with the single dynamic networks (Figure S2) indicate that the glass transition temperature, T_g, remains unchanged with the addition of metal ions. A secondary weak transition detected in the DSC traces is shifted to higher temperatures as the Cu-content increases. In the lack of evidence of clustering for ion amounts below 1.0eq. (from WAXS data not shown here [61]) this is attributed to the decrease of p_{dang} and the consequent slow-down of the dynamics upon addition of metals. Figure 3 shows that the single-ion transient networks do not obey the Cox-Merz empirical rule. In particular, the steady-state shear viscosity data lie above the complex viscosity data in the non-Newtonian regime. This deviation strongly depends on the stability of the metal-ligand interactions (persistent associations over long time), with a more pronounced failure of the Cox-Merz rule observed for stronger bonds. Indeed, while the steady-state viscosity of Zn(II) is slightly higher than the complex viscosity, the difference becomes more pronounced in the presence of (same amount of)

Cu (II) or Co (II). This observation is consistent with reference [23] (see also Figures 4 and 7 below) where the probability of a sticker to be free (p_{free}) for 0.5eq. Zn(II) is one order of magnitude larger than the one for 0.5eq. Cu (II) at 40°C.

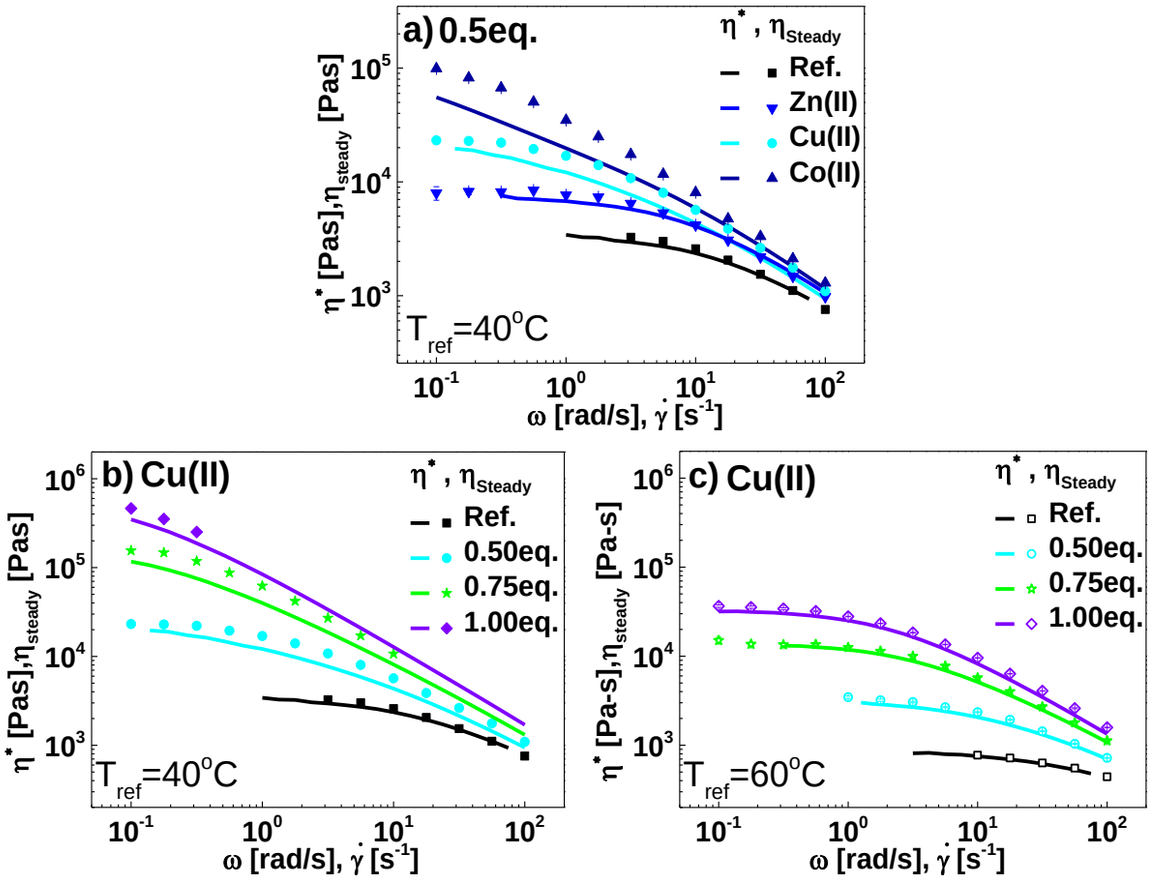

Figure 3. Cox-Merz rule representation for single dynamic networks with different (a) associating groups, (b) ion content and (c) temperature. Solid lines correspond to complex viscosities and symbols to steady-state viscosities. Error bars correspond to the size of the symbols.

Increasing the ion content, i.e., crosslinking density (Figure 3b), by changing the amount of available ions while keeping the other two parameters (ion type and temperature) constant, yields a stronger discrepancy between steady and dynamic viscosities. This suggests that upon adding an excess of ions, the number of dangling ends is reduced and consequently the network becomes less dynamic and is characterized by longer relaxation time (similarly to using stronger metal-ligand associations which lead to more stable networks). Note however that this is not evident at the

highest ion context of 1.0eq., where only a few steady shear data could be obtained (at rates below $0.5s^{-1}$) due to unavoidable edge fracture instabilities despite our efforts. We show this limited dataset to mark the limit of our measurement capabilities (still, the Cox-Merz is not valid here). The influence of temperature on the nonlinear dynamics can be appreciated by comparing Figures 3b and 3c. At higher temperature, the ligand exchange mechanism speeds-up and eventually the effect of sticker dynamics becomes negligible, leading to validation of the Cox-Merz rule. Further experimental evidence is presented in the collective plot of viscosity ratios (Figure S3) at the same rate or frequency. Same trend is found for all samples.

From the shear stress growth coefficient data of the different types of metal ions (Figure 4a), it is observed that close to the linear regime, the steady-state shear viscosity increases with increasing the lifetime of the metal-ligand complexes. This direct link between steady-state values and lifetime of the complexes is further highlighted in Figure 5b below, where all data collapse into a master curve when the stress is plotted against the Weissenberg number ($Wi = \dot{\gamma} \cdot \tau_d$). The latter is based on a characteristic time τ_d marking the onset of terminal relaxation in the linear viscoelastic spectrum and assigned to the inverse frequency at the moduli crossover. Therefore, for associating polymers such as the present telechelic stars, τ_d depends on the probability for a sticker to be dissociated [23]. On the other hand, at high shear rates, the steady-state viscosity is nearly independent of the metal ion (see Figure 4a). In this regime, the flow dominates and the time needed for the molecules to renew their environment is around $1/\dot{\gamma}$, whatever the strength of the reversible bonds may be. While the steady-state viscosities are similar, we observe that in this regime the overshoot of the shear stress growth coefficient strongly depends on the ion type and is more pronounced for stronger ions when the samples are deformed at the same conditions, i.e., same shear rate, temperature and ion content (Figure 4a). This reflects the enhanced ability of the network with stronger metal-ligand bonds to resist deformation before breakup and flow. In this context, a weak, albeit unambiguous upward deviation of the stress from the linear viscoelastic envelope (shear strain hardening) can be seen in Figure 4a. This is a common feature of associative polymers and is attributed to the slow disassociation kinetics of the metal-ligand complexes and the related larger resistance of trapped chain segments to detachment from associations [33–39]. The weak shear strain hardening seems to be more pronounced when the metal-ligand association becomes stronger, at intermediate time window.

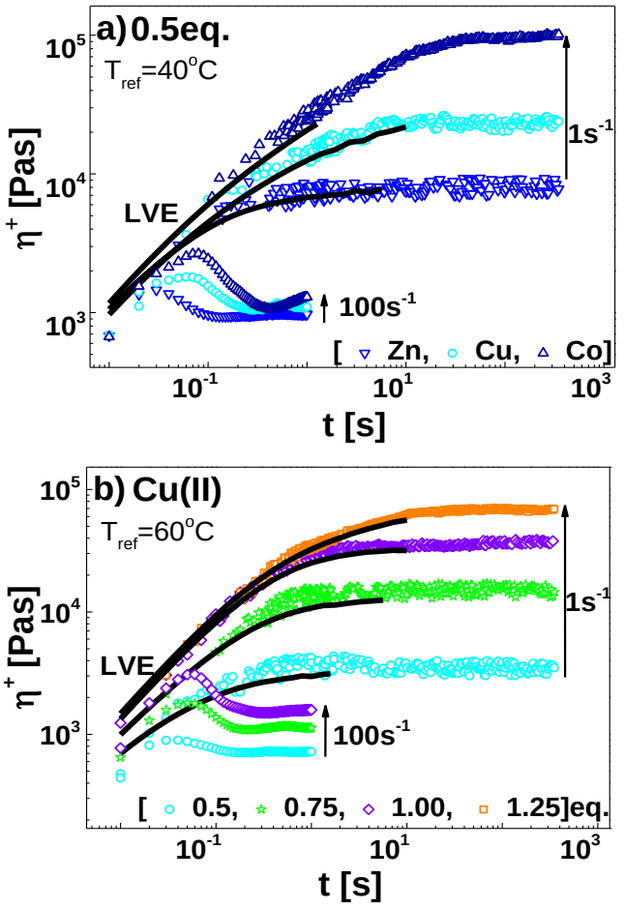

Figure 4. Shear stress growth coefficient of single dynamic networks with different (a) associations types at 40°C and (b) Cu-ion networks with increasing ion content at 60°C.

As shown in Figure 4b, the main features of the transient nonlinear response, i.e., shear strain hardening, overshoot of shear stress growth function and steady-state viscosity, appear enhanced as the crosslinking density of the transient networks increases. This can again be attributed to the enhanced stability of the transient network containing a larger amount of ions [23].

The steady-state viscosities of the different samples follow a universal trend when appropriately normalized (see Figure S4). It is found that for all types of ions and different stoichiometric amounts, the normalized steady-state viscosity (by the product of plateau modulus G_N^0 and τ_d) data collapse onto a universal curve when plotted against *Wi*, with a thinning slope of -0.76, at 40°C and 60°C. This slope is slightly higher compared to the respective value (-0.67) reported in the literature for entangled star polymers [62]. This is attributed to the broader range of

Weissenberg numbers reached with the dynamic networks, likely due to the interplay between disentanglement and breaking/re-association of bonds. In fact, the present data of the reference sample do not exceed a *Wi* value of 2.5 in Fig.S4, where the ultimate slope of -0.76 has not been reached.

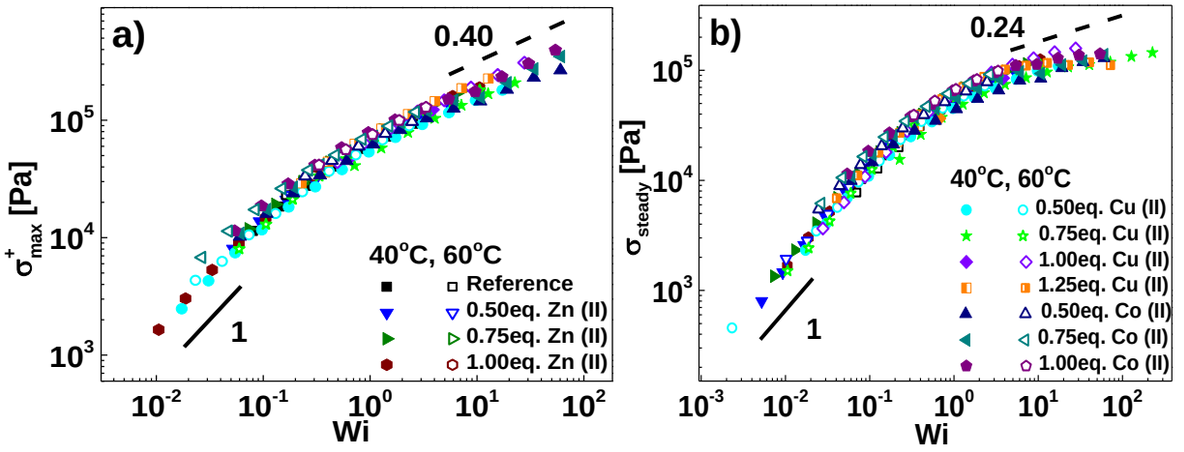

Figure 5. (a) Stress growth function overshoot and (b) Steady-state stress values as a function of the Weissenberg number for the reference sample and the single-ion networks at temperature 40°C and 60°C. The (common) legend is split in the two plots. See also respective viscosity plot of Figure S4.

As shown in Figure 5, both yield stress and steady-state stress superimpose when plotted as a function of *Wi*. The ability to build these master curves suggests that the shear properties of the transient networks are governed by the dynamics of the reversible stickers, which dictates how fast the star arms can move and disentangle/re-entangle. The overshoot is related to the orientation/stretching of the arms and the breakage of the dynamic bonds (see Figure 4). The steady-state stresses of the different samples as a function of *Wi* (Figure 5b) follow a universal slope of 1 for *Wi<1*, reflecting the predominance of terminal star-arm dynamics (taking place at the rhythm of the association/dissociation of the stickers). The slope becomes weaker (reaching a value of 0.24) at *Wi>1*, signaling the predominance of flow-induced disentanglement of the star-arms (for example, by convective constraint release). This is consistent with the results of Figure 4, which indicate that at high shear rates the steady-state viscosity is far less sensitive to the dynamics of the transient bonds.

In order to further highlight the relative resistance to deformation of the transient networks, Figure 6 depicts the shear stress growth function, shifted by a factor which is the ratio of steady-state stresses, $\frac{\sigma_{st,Cu}}{\sigma_{st,Zn,Cu,Co}(\dot{\gamma})}$, as a function of relative strain, for different association strengths (metals) and amounts of ions. In this figure, the data of sample Star250k-Cu-0.5eq. ($\sigma_{st,Cu}$) are taken as reference. The proposed shifting is motivated by the universal behavior of the steady-state stress versus *Wi* (see Figure 5b), which implies that in the steady-state regime, a sample characterized by a relaxation time τ_d and deformed at a rate $\dot{\gamma}$ behaves similarly to the reference sample, if the latter were deformed at an effective rate of $\frac{\tau_d}{\tau_{d,0.5eq\ Cu}}\dot{\gamma}$. In other words, $\sigma_{st,Zn,Cu,Co}(\dot{\gamma}) = \sigma_{st,Cu}\left(\frac{\tau_d}{\tau_{d,0.5eq\ Cu}}\dot{\gamma}\right)$. Therefore, in order to compare the viscoelastic response of a given sample with respect to that of the reference sample Star250k-Cu-0.5eq., we shift the shear stress growth function data (of samples containing Co (II) or Zn (II) ions) to compensate for their different effective rate (or equivalently, different dynamics), in a similar way the LVE data are shifted to build a master curve at a reference temperature [23]. This figure depicts data for three characteristic shear rates to facilitate the discussion. The complete dataset is depicted in Figure S5.

We observe that the overshoot of the shear stress growth function (which we call static yield stress) increases with shear rate and is higher for stronger networks (based on cobalt, Figure 6a) or larger degree of crosslinking (Figure 6b), in good agreement with the significant increase of the activation energy for breaking the associations, as quantified in the linear dynamics study of these networks [23]. We also observe that with the most stable complexes, at high shear rates and at 40°C (Figure 6a), the shear stress growth function displays a broad overshoot, whose peak is delayed compared to the network containing Zn(II) ions. The shape of the overshoot of the latter network is similar to that of an entangled star polymer, with a maximum appearing immediately after the elastic regime of deformation and the respective strain reaching a value of about 2 (see Figure 8 below). While in the presence of Cu(II) or Co(II) ions, the shear stress growth function starts to bend at a similar strain value as with the Zn(II) network, it increases further to reach a maximum at a strain of around 6 (as discussed below, see Figure 8). Hence, the regime extending from the bending of the shear stress growth function to its steady state is distinct for each metal. This suggests that these networks are able to sustain much larger deformation before breaking, presumably because of the larger strength of their supramolecular bonds: while the shifted curves of Figure 6 account

for the different overall dynamics of the reversible junctions, which governs the steady-state stress (the steady-state data collapse), they do not account for the different strength (or ability to resist to a deformation) of the metal-ions complexes. Once broken under shear, the reversible bonds have the ability to re-associate and thus, a higher steady-state viscosity is reached (see failure of the Cox-Merz rule). Depending on the strength of the metal-ligand association and degree of re-association, a weak second overshoot might appear at longer times and higher shear rates.

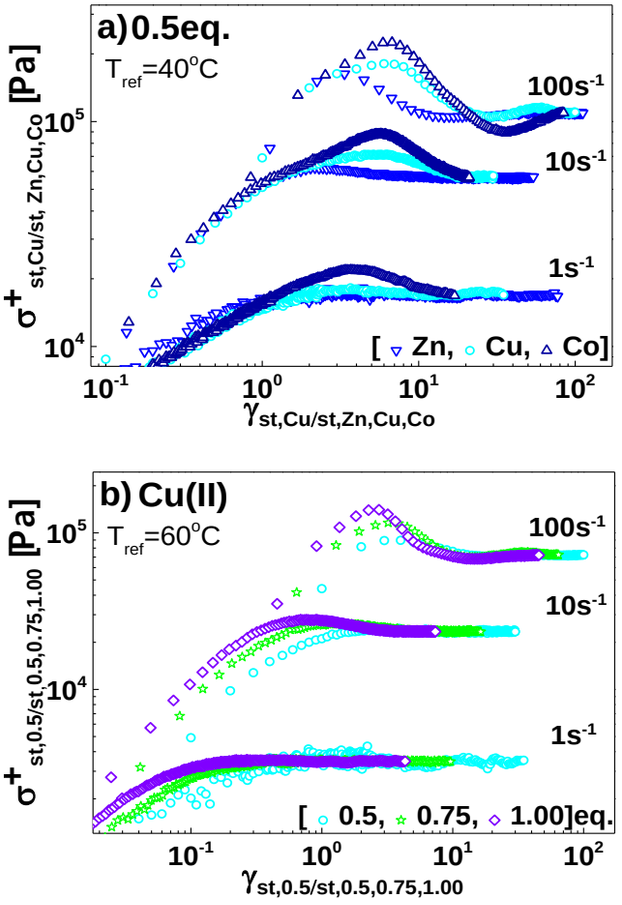

Figure 6. Shifted shear stress growth function versus shifted strain (with respect to a reference value, see text) of single dynamic networks with (a) different association types at 40°C and (b) Cu-ion networks with varying crosslinking density at 60°C.

The delay of the maximum in shear stress growth function depends on temperature. This is observed in Figure 6b, which shows that when the network containing 0.5eq. Cu(II) is heated at 60°C, the maximum disappears (at 1 and 10 s^{-1}) or is shifted to a lower yield strain (at 100 s^{-1}). It is also observed that increasing the amount of ions reinforces the network (enhanced overshoot)

and decreases the proportion of dangling ends (larger elasticity at short time), in agreement with the analysis of the linear viscoelastic properties of these samples [23].

The analysis of the shape of the shear stress growth function overshoot can also provide additional insights about the recombination of bonds that break at the yield point. Increasing the ion content leads to a change in the shape of the overshoot (Figure S6a, b). This conforms to the larger stress overshoot and implies enhanced elastic deformation before break, hence faster recovery. Actually, the broadness of the overshoot (expressed as the width at half height) does not seem to strongly depend on ion content but it does depend on the imposed shear rate, suggesting that the flow-induced break-up of bonds affects the structure and possibly the homogeneity of the transient networks (Figure S6c).

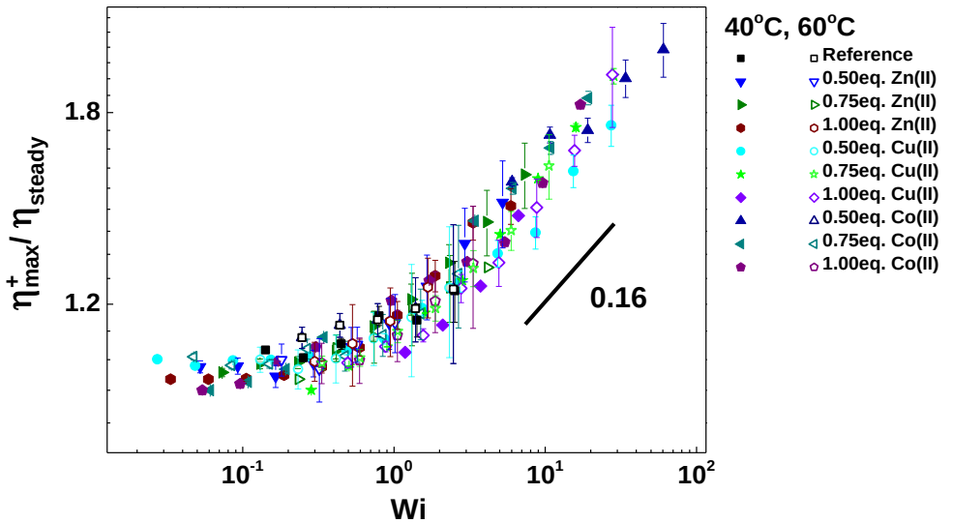

Figure 7. Fractional viscosity overshoot as a function of Weissenberg number for all dynamic networks, at two different temperatures (40°C and 60°C). The slope is consistent with those of shear stress growth function and steady-state stress in Figure 5.

The fractional viscosity overshoot is plotted against the Weissenberg number in Figure 7 for the single dynamic networks at different compositions and temperatures. As expected from Figure 6, we can observe that virtually all data collapse. Fractional viscosity overshoot may be thought of as a measure of mechanical coherence (extend of deformation exceeding its steady-state value), hence the investigated samples are similar in this respect when compared at the same *Wi*. The

present networks seem to exhibit an enhanced mechanical coherence (slope of 0.16) compared to entangled star polymers without stickers (slope of 0.05) consistent with the limited data of the reference sample, while they exhibit a larger yield stress [62]. When the shear rate increases, the sticker dynamics (and subsequent diffusion of the stars) becomes slow compared to $1/\dot{\gamma}$. Therefore, the transient network does not have time to reorganize its configuration in flow, and consequently it deforms and stretches, leading to a larger fractional viscosity overshoot. The faster the network is deformed, the larger the deformation before break, hence the larger is the overshoot.

Interestingly, the analysis of the strain at the overshoot, γ_{max} (which we call hereafter yield strain), as a function of *Wi* (Figure 8) reveals that it is independent of *Wi*. This threshold value of (saturated) elasticity, beyond which the network breaks, characterizes in general yield stress materials, which flow under mechanical load [63]. Accumulation of strain indicates that a certain fraction of the bonds remains unchanged during deformation, up to the yield point. As already mentioned, for networks formed by weaker Zn(II) ions, such strain accumulation is not observed as the bis-complexes do not resist flow appreciably. Indeed, the experimental data show that the weakly associated networks exhibit a predominantly polymeric response, characterized by segmental orientation (as per Doi-Edwards) and then chain stretching at $Wi>1$ with a slope of 0.33 for entangled polymers [64], similarly to the behavior of the reference sample. Interestingly, the weakest network with largest fraction (1.0eq.) of Zn(II) ions exhibits a stronger *Wi*-dependence. However, the data are too limited to draw more definite conclusions at present concerning the possible interplay of chain (star arm) stretching and association/dissociation exchange. It should be noted that the stronger networks with saturated γ_{max} of about 6, also contain a small fraction of network strands which are not trapped (with metal-ligand associations) and are unable to sustain high deformations. However, they do not dominate the response of these networks.

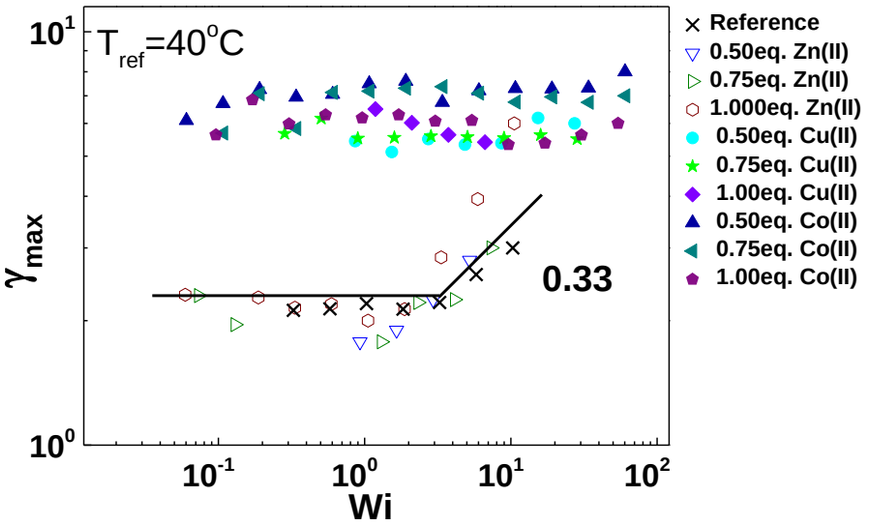

Figure 8. Strain at overshoot (yield) as a function of the Weissenberg number for all single transient networks and the reference sample at 40°C. The solid line indicates the 2.3 Doi-Edwards value and the line with 0.33 slope observed for entangled neutral polymers at high Weissenberg numbers due to stretching. The weaker Zn-ions are indicated by open symbols. The reference (neutral) sample is marked by "X".

Previous studies found the yield strain to increase logarithmically with shear rate in dynamic networks [40–42]. Skrzeszewska et al. [43] modeled this response by accounting for enhanced bond rupture kinetics with shear rate. On the other hand, strain accumulation up to its maximum has been observed in the numerical studies of Koga and co-workers, who used the non-affine transient network theory to explain the nonlinear shear rheology of self-assembled telechelic polymer solutions [37]. These solutions exhibited shear strain hardening and a virtually constant maximum strain accumulation. The latter was attributed to two factors, the coupling between disassociation rate and chain tension (which is a measure of how easily chains are effectively detached from the micelles formed by self-assembly, hence it involved chain tension) and the chain nonlinearity (its departure from Gaussian conformation, which reflects eventual chain stretch). It turns out that the combination of these factors resulted in a very weak dependence of γ_{max} on *Wi*, as observed with our system.

B. Double lifetime networks

The shear stress growth coefficient of DDNs with Zn and Cu at 0.50eq. and 1.0eq. contents is depicted in Figure 9 at selected shear rates and temperature. The use of CPP enables reliable measurements at high shear rates, as confirmed by the reproducible linear viscoelastic measurements after each shear transient test (see also Figure S7).

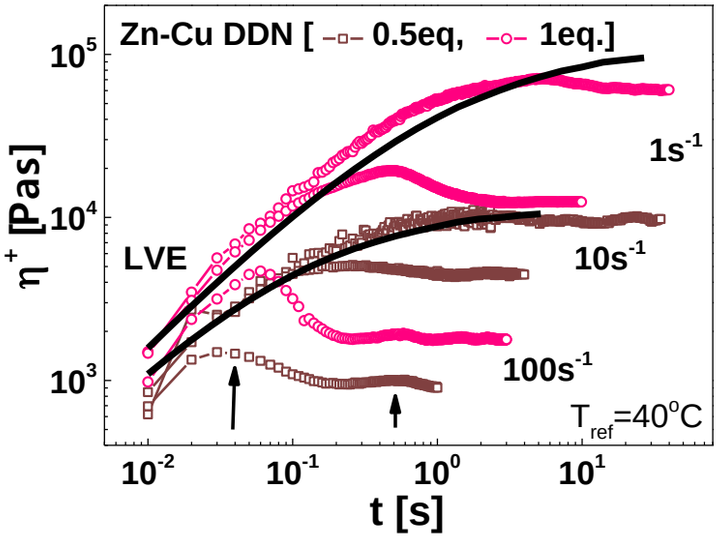

Figure 9. Comparison of shear stress growth coefficient data at the same rates and temperature for double dynamics network based on Cu and Zn groups with 0.5eq. (squares) and 1.0eq. (circles) ion content. The vertical arrows indicate the two overshoots (see text).

Similarly to the case of single lifetime networks (Figure 4), increasing the crosslinking density by adding an excess of metal-ions in the double dynamics networks enhances the steady-state viscosity at the same shear rate. This is consistent with the longer relaxation time of the double dynamics network containing 1.0eq. ions [23], or equivalently with their higher complex viscosity (Figure S8). It is also in agreement with the fact that the steady-state stress, which depends on *Wi*

(see also Figure 6b), is governed by the sticker dynamics. However, contrary to the single dynamic networks, which exhibit a yield strain value of either 2 or around 6, independently of the amount of ions (Figure 8), we see here an enhancement of the shear stress growth coefficient signal, with its maximum being shifted from a strain value of 2 with 0.5eq. ions to 6 with 1.0eq. ions (Figure S9). Based on the compiled data of Figure 8, this suggests that the viscoelastic response of the blends shifts from a Zn(II)-dominated network to a Cu(II)-dominated network with increasing the amount of ions and shear rate. It is also observed that the shear strain hardening at $10s^{-1}$ appears to be stronger for the double dynamics network with higher crosslinking density, similarly to the Cu(II) single dynamic networks, which has a more pronounced strain hardening compared to Zn(II) (Figure 4a). From the viscoelastic data of the two samples, same conclusions can be drawn (Figure S8). Actually, the magnitude of the activation energy for the double dynamics network with 1.0eq. of Zn-ions and Cu-ions is nearly identical to that of the respective single dynamic network with Cu-ions [23]. However, despite the fact that with 1.0eq. amount of ions the double dynamics network behaves akin to the single dynamic Cu(II) network, we remark that the latter could not be sheared at rates above $0.32s^{-1}$ (it could not resist larger deformation, see Figure 3b), while on the contrary, the double dynamics network could be deformed up to very high shear rates and eventually flow (Figures S9,S10). This suggests that the addition of weaker ions within the Cu(II) network brings the necessary local mobility (analogous to the so-called sacrificial bonds), so that the network can quickly adapt to a large deformation, while the presence of Cu(II) ions ensures the sample to keep its larger coherence (or resistance to deformation), with a yield strain of 6. Hence, the double dynamics reflect a dynamic coupling of the weakly and strongly associating components. There seems to be an interesting qualitative analogy with the mechanism of DN deformation put forth by Gong et al. [46, 52], according to which one network is more vulnerable to stretching (sacrificial), with the other network being more resistant, hence providing large deformability and coherence to the overall material [47]. In the present situation, instead of covalent bonds, the 'stiff' component of the DDNs forms stronger (reversible) bonds. Such an approach has been reported so far for hydrogels with self-healing properties [54–55], but not in the context of transient shear rheology in the melt state. On the other hand, the weaker single dynamic Zn(II)-complexes break macroscopically when deformed at a rate of $177s^{-1}$ or higher, i.e., much before the DDNs.

Figure 9 also shows that a second weak overshoot (indicated by arrow) emerges in the shear stress growth coefficient signal in the strongly nonlinear regime ($100s^{-1}$). The unambiguous appearance of two overshoots is confirmed by careful account of different experimental issues, repeat measurements and the reproducible linear viscoelastic measurements following the nonlinear tests (see Figures S1b and S8). The first overshoot is very similar to that of the single dynamic networks, while the second overshoot reflects predominantly the response of the Cu(II)-ion complexes. In the presence of stronger metal-ligand complexes, the chain segments can deform substantially more than those associated with the (sacrificial) weaker Zn(II) complexes (however, this depends on the ion content as discussed below).

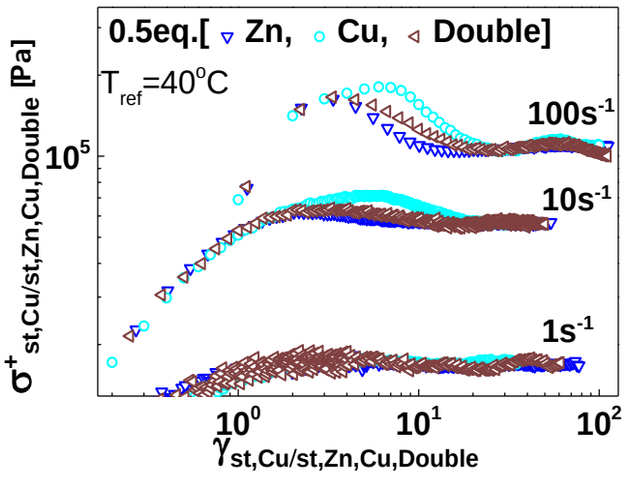

Figure 10. Shifted shear stress growth function versus shifted strain (as in Figure 6) of single dynamic supramolecular polymers and the resulting double dynamics network with 0.50eq. [Zn (II) + Cu(II)] at 40°C.

Figure 10 is equivalent to Figure 6 and examines the relative resistance of the double dynamics networks to deformation by comparing the shifted shear stress growth functions of the DDN with its respective single dynamic networks, at 0.5eq. ions. It can be observed that the steady-state response of all networks is virtually identical at low rates ($1s^{-1}$). With increasing shear rate to $10s^{-}$

[1], the DDN response remains similar to that of the single dynamic Zn(II)-network (see also the original, unshifted data of Figure S9), however that of the Cu(II)-network becomes distinct. This is more evident at the highest shear rate ($100s^{-1}$) where at intermediate relative strains (between the two overshoots) the DDN data are between those of the two single dynamic networks. In fact, with increasing shear rate the appearance of the weak second overshoot becomes evident (see also Figures 9 and S9a). Concerning the first overshoot at $100s^{-1}$, the respective value of the shifted strain for the DDN is about 3, very similar to that of the Zn(II)-network and smaller than that of the Cu(II)-network (6). However, the DDN overshoot is much broader (see Figure S11). This behavior is also consistent with Figure S9. Comparison of Figures 10, S7a, S9 and S10 suggests that at higher ion content, the stronger and longer-living Cu(II)-complexes dominate over the weaker Zn(II)-complexes and the response of the double dynamics network resembles that of the single dynamic Cu(II)-complex network, however with weaker shear stress growth function (see Figures S9b and S10 for 1.0eq.). In this respect, the weaker Zn-ion component is indeed sacrificial at sufficiently high ion content. The emerging nonlinear behavior of the DDNs is consistent with the analysis of their linear viscoelasticity. Indeed, it was revealed quantitatively that the delay of the arm disentanglement induced by the dynamics of the reversible junctions (and taken into account with the parameter p_{free}) for DDNs comprising Zn-ions and Cu-ions, gradually shifts from a delay similar to single dynamic Zn-ion network towards that of the single dynamic Cu-ion network with increasing ion content [23].

Concerning the emergence of a second overshoot in the stress growth function at high shear rates, the interplay of association strength and chain deformation in a broader sense, discussed in the context of single dynamic networks [37] seems to be at the origin of the observed response. We speculate that the two groups with different strengths contribute to two distinct dynamic processes that govern the overall rheological signal of the double dynamics network. In this context, we recall that comb polymers exhibiting hierarchical relaxation starting with branches, followed by backbone [65], and binary non-associating entangled polymer melts with two different relaxation modes [66] were found to exhibit a second overshoot in the shear stress growth coefficient at large shear rates. Concerning the latter, polystyrene solutions with bimodal molecular weight distributions studied by Osaki and co-workers exhibited a double overshoot when the stretch time (identified by the Rouse relaxation time) of the larger component exceeded the terminal time of

the shorter one [67]. In analogy to that result, we remark that the second overshoot in DDNs emerges after steady-state stress following the first overshoot (Figures 9, 10, S9).

The validity of the Cox-Merz rule depends on ion content and temperature. For example, the rule is validated for DDNs with 0.5eq. of Zn-ions and Cu-ions at 60°C, but not at 40°C or for 0.5eq. of Zn-ions and Co-ions at 60°C. However, the discrepancy between dynamic and steady-shear data is weaker for these DDNs when compared to respective strong single components (Figures 3 and S8). We attribute this to the fact that DDNs have the weaker component (Zn-ions) whose respective weak single dynamic network obeys the Cox-Merz rule.

The combination of DDN properties pertaining to fractional viscosity overshoot (with much stronger dependence on *Wi* compared to single dynamic networks) and shear thinning behavior (Figure 11) suggests their enhanced mechanical coherence and deformability (see strong dependence on Wi with slope of 0.24). Judicious choice of the ions provides possibilities to tailor the mechanical properties in this class of materials.

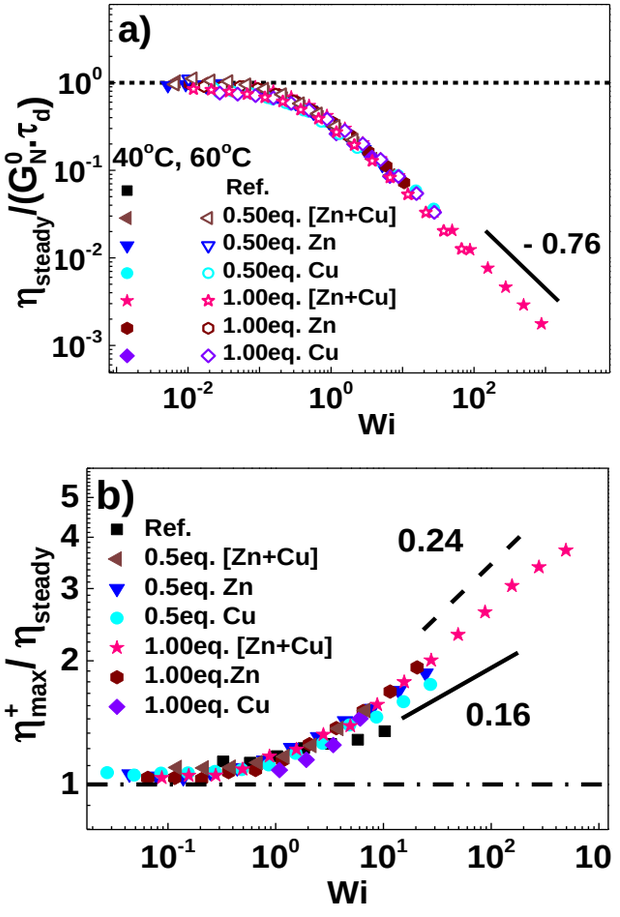

Figure 11. Normalized steady-state shear viscosities (a) and fractional viscosity overshoot (b) as a function of the Weissenberg number for DDNs made of Zn-ions and Cu-ions. The data of the respective single dynamic network components are also shown in the plots.

The above discussion renders a comment on the presence of dangling arms (free ligands) necessary. This important point was addressed in the context our modeling analysis of the linear viscoelasticity of the DDNs [23]. In that work, the proportion of dangling ends was estimated from the value of the rubbery plateau modulus. A large fraction of dangling ends was found, which decreased when the amount of metal ions increased from 0.5eq., 0.75eq., 1.0eq., to 1.25eq.. This result was validated by comparing the FTIR absorption spectrum of the reference sample (Star250k-tpy4) to that of a pure, unfunctionalized linear PnBA (with weight-average molar mass M_w = 26kg/mol), which led us to assign the absorption bands corresponding to the vibrations of the terpyridine groups [68–69] and determine the proportion of associated versus free terpyridines. In fact, even at 0.75eq. of metal ions, i.e., above the stoichiometric amount for Zn(II), the presence of non-coordinated ligand was identified, consistently with the assumption of the presence of dangling ends. We believe that the combination of very large molar mass of the star molecules used here and very low amount of metal ions explains the presence of free ligands in our networks at stoichiometric conditions (or slightly beyond). Clearly however, the more ions are added into the system, the less significant is the fraction of these unassociated arms.

Finally, a note on the possible use of UV titration tests to determine the proportion of metal-ligand complexes is in order. This technique can indeed be used to detect the formation of the metal-ligand complexes. In fact, the degree of functionalization of telechelic four-arm Star250k-tpy4 was assessed by UV-visible titration with metal cations (Fe^{2+}, which gives rise to a strong absorption in the visible region), which yields a functionality of 97±3%, suggesting that almost the entirety of the chains are end-functionalized with the terpyridine group [61]. However, the proportions of metal-ligand complexes determined from the equilibrium constants are of qualitative value only since they were obtained in solution. Moreover, in the melt state the star molecules are entangled, their mobility is largely reduced compared to solutions, and this also affects the association/dissociation dynamics of the metal-terpyridine complexes [23].

CONCLUSIONS

The detailed experimental investigation of the nonlinear shear response of single and double dynamics networks based on different metal-ligand associations has revealed a number of interesting features. The single dynamic networks do not obey the Cox-Merz rule, with this failure being more pronounced for stronger associations, exhibit shear thinning viscosity which is weaker than that of entangled neutral polymers (having a universal shear thinning exponent of -0.76), weak shear strain hardening and substantial mechanical coherence (enhanced fractional viscosity overshoot and stronger shear rate dependence compared to neutral polymers). The shear stress growth function is characterized by an overshoot which is enhanced with increasing strength and concentration of bonds as well as shear rate, while a second weak overshoot appears at high rates and higher ion content.

The double dynamics networks exhibit similar features to the single dynamic networks, but with some notable quantitative differences: less pronounced failure of the Cox-Merz rule, enhanced mechanical coherence, larger accumulated strain in steady-state flow, same universal shear thinning viscosity, stronger shear strain hardening that is further enhanced at high shear rates, and double overshoot reflecting the distinct contributions of the individual metal-ion complexes. These properties of the double dynamics networks by be rationalized by invoking the concept of sacrificial bonds, put forth in the context of double networks comprising one permanent and one dynamic network at sufficiently high ion content. In this respect, the sacrificial component of the DDNs is that with the weaker bond (Zn-ions), which provides local energy dissipation and enhances the overall deformability of the material. Further, the fact that the nonlinear shear properties of DDNs appear to interpolate between the respective properties of the two constituents reflects similarities with their linear viscoelastic response. The latter is characterized by a delay of arm disentanglement due to the reversible bonds, which has been shown to effectively interpolate between the two single dynamic network components, depending on composition.

Ion content, strength of associations and temperature (which affects the strength) are the key parameters influencing the nonlinear rheology of these metal-ligand networks over a wide range of Weissenberg numbers covering three decades. In addition, the molar mass and macromolecular architecture of the polymeric precursor should play a crucial role in tailoring properties, but this is

not addressed in the present study. Hence, the present dataset provides possibilities to tailor the rheology of this class of polymeric network materials by choosing or altering the ions type and content.

ACKNOWLEDGEMENTS

Financial support by the EU (Horizon 2020, Marie Skłodowska-Curie ITN DoDyNet, Grand Agreement No. 765811) is gratefully acknowledged. We thank E. Glynos, R. Xie and R. H. Colby for help the DSC and WAXS measurements. E.V.R. is Senior Research Associate of the FRS-FNRS.

REFERENCES

[1] L. Brunsveld, B. J. B. Folmer, E. W. Meijer, & R. P. Sijbesma, "Supramolecular Polymers," Chemical Reviews, **101** (2001) 4071–4098. https://doi.org/10.1021/cr990125q.
[2] G. T. Williams, C. J. E. Haynes, M. Fares, C. Caltagirone, J. R. Hiscock, & P. A. Gale, "Advances in applied supramolecular technologies", Chemical Society Reviews, **50** (2021) 2737–2763. https://doi.org/10.1039/D0CS00948B.
[3] E. Vereroudakis & D. Vlassopoulos, "Tunable dynamic properties of hydrogen-bonded supramolecular assemblies in solution", Progress in Polymer Science, **112** (2021) 101321. https://doi.org/10.1016/j.progpolymsci.2020.101321.
[4] P. Lavrador, M. R. Esteves, V. M. Gaspar, & J. F. Mano, "Stimuli-Responsive Nanocomposite Hydrogels for Biomedical Applications", Advanced Functional Materials, **31** (2021) 2005941. https://doi.org/10.1002/adfm.202005941.
[5] Q. He, Y. Zhang, H. Li, & Q. Chen, "Rheological Properties of ABA-Type Copolymers Physically End-Cross-Linked by Polyoxometalate", Macromolecules, **53** (2020) 10927–10941. https://doi.org/10.1021/acs.macromol.0c01817.
[6] H. Yang, S. Wu, & Q. Chen, "How to Choose a Secondary Interaction to Improve Stretchability of Associative Polymers?", Macromolecules, **54** (2021) 8112–8121. https://doi.org/10.1021/acs.macromol.1c01283.
[7] J. Suzuka, M. Tsuda, L. Wang, S. Kohsaka, K. Kishida, S. Semba, H. Sugino, S. Aburatani, M. Frauenlob, T. Kurokawa, S. Kojima, T. Ueno, Y. Ohmiya, H. Mano, K. Yasuda, J. P. Gong, & S. Tanaka, "Rapid reprogramming of tumour cells into cancer stem cells on double-network hydrogels", Nature Biomedical Engineering, (2021) 1–12. https://doi.org/10.1038/s41551-021-00692-2.

[8] C. Heinzmann, S. Coulibaly, A. Roulin, G. L. Fiore, & C. Weder, "Light-Induced Bonding and Debonding with Supramolecular Adhesives", ACS Applied Materials & Interfaces, **6** (2014) 4713–4719. https://doi.org/10.1021/am405302z.

[9] S. Bode, L. Zedler, F. H. Schacher, B. Dietzek, M. Schmitt, J. Popp, M. D. Hager, & U. S. Schubert, "Self-Healing Polymer Coatings Based on Crosslinked Metallosupramolecular Copolymers", Advanced Materials, **25** (2013) 1634–1638. https://doi.org/10.1002/adma.201203865.

[10] Y.-L. Rao, A. Chortos, R. Pfattner, F. Lissel, Y.-C. Chiu, V. Feig, J. Xu, T. Kurosawa, X. Gu, C. Wang, M. He, J. W. Chung, & Z. Bao, "Stretchable Self-Healing Polymeric Dielectrics Cross-Linked Through Metal–Ligand Coordination", Journal of the American Chemical Society, **138** (2016) 6020–6027. https://doi.org/10.1021/jacs.6b02428.

[11] T. Tomkovic & S. G. Hatzikiriakos, "Nonlinear rheology of poly(ethylene-co-methacrylic acid) ionomers", Journal of Rheology, **62** (2018) 1319–1329. https://doi.org/10.1122/1.5042521.

[12] Q. Chen, G. J. Tudryn, & R. H. Colby, "Ionomer dynamics and the sticky Rouse model", Journal of Rheology, **57** (2013) 1441–1462. https://doi.org/10.1122/1.4818868.

[13] M. Rubinstein & A. N. Semenov, "Dynamics of Entangled Solutions of Associating Polymers", Macromolecules, **34** (2001) 1058–1068. https://doi.org/10.1021/ma0013049.

[14] C. Schaefer, P. R. Laity, C. Holland, & T. C. B. McLeish, "Silk Protein Solution: A Natural Example of Sticky Reptation", Macromolecules, **53** (2020) 2669–2676. https://doi.org/10.1021/acs.macromol.9b02630.

[15] D. Bedrov, G. D. Smith, & J. F. Douglas, "Influence of self-assembly on dynamical and viscoelastic properties of telechelic polymer solutions", EPL (Europhysics Letters), **59** (2002) 384–390. https://doi.org/10.1209/epl/i2002-00206-0.

[16] E. van Ruymbeke, D. Vlassopoulos, M. Mierzwa, T. Pakula, D. Charalabidis, M. Pitsikalis, & N. Hadjichristidis, "Rheology and Structure of Entangled Telechelic Linear and Star Polyisoprene Melts", Macromolecules, **43** (2010) 4401–4411. https://doi.org/10.1021/ma902769s.

[17] V. Metri, A. Louhichi, J. Yan, G. P. Baeza, K. Matyjaszewski, D. Vlassopoulos, & W. J. Briels, "Physical Networks from Multifunctional Telechelic Star Polymers: A Rheological Study by Experiments and Simulations", Macromolecules, **51** (2018) 2872–2886. https://doi.org/10.1021/acs.macromol.7b02613.

[18] M. Zuliki, S. (张世岭) Zhang, T. Tomkovic, & S. G. Hatzikiriakos, "Capillary flow of sodium and zinc ionomers", Physics of Fluids, **32** (2020) 023106. https://doi.org/10.1063/1.5145303.

[19] M. Zuliki, S. Zhang, K. Nyamajaro, T. Tomkovic, & S. G. Hatzikiriakos, "Rheology of sodium and zinc ionomers: Effects of neutralization and valency", Physics of Fluids, **32** (2020) 023104. https://doi.org/10.1063/1.5142563.

[20] A. Shabbir, Q. Huang, G. P. Baeza, D. Vlassopoulos, Q. Chen, R. H. Colby, N. J. Alvarez, & O. Hassager, "Nonlinear shear and uniaxial extensional rheology of polyether-ester-sulfonate copolymer ionomer melts", Journal of Rheology, **61** (2017) 1279–1289. https://doi.org/10.1122/1.4998158.

[21] A. Shabbir, Q. Huang, Q. Chen, R. H. Colby, N. J. Alvarez, & O. Hassager, "Brittle fracture in associative polymers: the case of ionomer melts", Soft Matter, **12** (2016) 7606–7612. https://doi.org/10.1039/C6SM01441K.

[22] F. Zhuge, L. G. D. Hawke, C.-A. Fustin, J.-F. Gohy, & E. van Ruymbeke, "Decoding the linear viscoelastic properties of model telechelic metallo-supramolecular polymers", Journal of Rheology, **61** (2017) 1245–1262. https://doi.org/10.1122/1.4997593.

[23] Y. Li, C. Pyromali, F. Zhuge, C.-A. Fustin, J.-F. Gohy, D. Vlassopoulos, & E. Van Ruymbeke, "Dynamics of entangled metallo-supramolecular polymer networks combining stickers with different lifetimes", Journal of Rheology, (2021).

[24] M. Ahmadi, L. G. D. Hawke, H. Goldansaz, & E. van Ruymbeke, "Dynamics of Entangled Linear Supramolecular Chains with Sticky Side Groups: Influence of Hindered Fluctuations", Macromolecules, **48** (2015) 7300–7310. https://doi.org/10.1021/acs.macromol.5b00733.

[25] L. Pellens, R. Gamez Corrales, & J. Mewis, "General nonlinear rheological behavior of associative polymers", Journal of Rheology, **48** (2004) 379–393. https://doi.org/10.1122/1.1645517.

[26] Y. Caram, F. Bautista, J. E. Puig, & O. Manero, "On the rheological modeling of associative polymers", Rheologica Acta, **46** (2006) 45–57. https://doi.org/10.1007/s00397-005-0066-y.

[27] S. Suzuki, T. Uneyama, & H. Watanabe, "Concentration Dependence of Nonlinear Rheological Properties of Hydrophobically Modified Ethoxylated Urethane Aqueous Solutions", Macromolecules, **46** (2013) 3497–3504. https://doi.org/10.1021/ma400429y.

[28] R. J. English, S. R. Raghavan, R. D. Jenkins, & S. A. Khan, "Associative polymers bearing n-alkyl hydrophobes: Rheological evidence for microgel-like behavior", Journal of Rheology, **43** (1999) 1175–1194. https://doi.org/10.1122/1.551026.

[29] J. Mewis, B. Kaffashi, J. Vermant, & R. J. Butera, "Determining Relaxation Modes in Flowing Associative Polymers Using Superposition Flows", Macromolecules, **34** (2001) 1376–1383. https://doi.org/10.1021/ma000987p.

[30] T. Annable, R. Buscall, R. Ettelaie, & D. Whittlestone, "The rheology of solutions of associating polymers: Comparison of experimental behavior with transient network theory", Journal of Rheology, **37** (1993) 695–726. https://doi.org/10.1122/1.550391.

[31] D. Xu & S. L. Craig, "Multiple Dynamic Processes Contribute to the Complex Steady Shear Behavior of Cross-Linked Supramolecular Networks of Semidilute Entangled Polymer Solutions", The Journal of Physical Chemistry Letters, **1** (2010) 1683–1686. https://doi.org/10.1021/jz1004818.

[32] T. A. Witten & M. H. Cohen, "Crosslinking in shear-thickening ionomers", Macromolecules, **18** (1985) 1915–1918. https://doi.org/10.1021/ma00152a019.

[33] S. Suzuki, T. Uneyama, T. Inoue, & H. Watanabe, "Nonlinear Rheology of Telechelic Associative Polymer Networks: Shear Thickening and Thinning Behavior of Hydrophobically Modified Ethoxylated Urethane (HEUR) in Aqueous Solution", Macromolecules, **45** (2012) 888–898. https://doi.org/10.1021/ma202050x.

[34] V. A. H. Boudara & D. J. Read, "Stochastic and preaveraged nonlinear rheology models for entangled telechelic star polymers", Journal of Rheology, **61** (2017) 339–362. https://doi.org/10.1122/1.4974908.

[35] G. W. Park & G. Ianniruberto, "A new stochastic simulation for the rheology of telechelic associating polymers", Journal of Rheology, **61** (2017) 1293–1305. https://doi.org/10.1122/1.4997592.

[36] T. Inoue, Y. Inoue, & H. Watanabe, "Nonlinear Rheology of CTAB/NaSal Aqueous Solutions: Finite Extensibility of a Network of Wormlike Micelles", Langmuir, **21** (2005) 1201–1208. https://doi.org/10.1021/la048292v.

[37] T. Koga, F. Tanaka, I. Kaneda, & F. M. Winnik, "Stress Buildup under Start-Up Shear Flows in Self-Assembled Transient Networks of Telechelic Associating Polymers†", Langmuir, **25** (2009) 8626–8638. https://doi.org/10.1021/la804227u.

[38] Y. Séréro, V. Jacobsen, J.-F. Berret, & R. May, "Evidence of Nonlinear Chain Stretching in the Rheology of Transient Networks", Macromolecules, **33** (2000) 1841–1847. https://doi.org/10.1021/ma991349d.

[39] D. Amin & Z. Wang, "Nonlinear rheology and dynamics of supramolecular polymer networks formed by associative telechelic chains under shear and extensional flows", Journal of Rheology, **64** (2020) 581–600. https://doi.org/10.1122/1.5120897.

[40] T. Yan, K. Schröter, F. Herbst, W. H. Binder, & T. Thurn-Albrecht, "Unveiling the molecular mechanism of self-healing in a telechelic, supramolecular polymer network", Scientific Reports, **6** (2016) 32356. https://doi.org/10.1038/srep32356.

[41] T. Yan, K. Schröter, F. Herbst, W. H. Binder, & T. Thurn-Albrecht, "What Controls the Structure and the Linear and Nonlinear Rheological Properties of Dense, Dynamic Supramolecular Polymer Networks?", Macromolecules, **50** (2017) 2973–2985. https://doi.org/10.1021/acs.macromol.6b02507.

[42] Q. Zhang, X. Zhu, C.-H. Li, Y. Cai, X. Jia, & Z. Bao, "Disassociation and Reformation Under Strain in Polymer with Dynamic Metal–Ligand Coordination Cross-Linking", Macromolecules, **52** (2019) 660–668. https://doi.org/10.1021/acs.macromol.8b02414.

[43] P. J. Skrzeszewska, J. Sprakel, F. A. de Wolf, R. Fokkink, M. A. Cohen Stuart, & J. van der Gucht, "Fracture and Self-Healing in a Well-Defined Self-Assembled Polymer Network", Macromolecules, **43** (2010) 3542–3548. https://doi.org/10.1021/ma1000173.

[44] N. Ghahramani, K. A. Iyer, A. K. Doufas, & S. G. Hatzikiriakos, "Rheology of thermoplastic vulcanizates (TPVs)", Journal of Rheology, **64** (2020) 1325–1341. https://doi.org/10.1122/8.0000108.

[45] E. Vereroudakis, M. Bantawa, R. P. M. Lafleur, D. Parisi, N. M. Matsumoto, J. W. Peeters, E. Del Gado, E. W. Meijer, & D. Vlassopoulos, "Competitive Supramolecular Associations Mediate the Viscoelasticity of Binary Hydrogels", ACS Central Science, **6** (2020) 1401–1411. https://doi.org/10.1021/acscentsci.0c00279.

[46] T. L. Sun, T. Kurokawa, S. Kuroda, A. B. Ihsan, T. Akasaki, K. Sato, M. A. Haque, T. Nakajima, & J. P. Gong, "Physical hydrogels composed of polyampholytes demonstrate high toughness and viscoelasticity", Nature Materials, **12** (2013) 932–937. https://doi.org/10.1038/nmat3713.

[47] E. Filippidi, T. R. Cristiani, C. D. Eisenbach, J. H. Waite, J. N. Israelachvili, B. K. Ahn, & M. T. Valentine, "Toughening elastomers using mussel-inspired iron-catechol complexes", Science, **358** (2017) 502–505. https://doi.org/10.1126/science.aao0350.

[48] A. A. Aldana, S. Houben, L. Moroni, M. B. Baker, & L. M. Pitet, "Trends in Double Networks as Bioprintable and Injectable Hydrogel Scaffolds for Tissue Regeneration", ACS Biomaterials Science & Engineering, (2021). https://doi.org/10.1021/acsbiomaterials.0c01749.

[49] D. R. King, T. Okumura, R. Takahashi, T. Kurokawa, & J. P. Gong, "Macroscale Double Networks: Design Criteria for Optimizing Strength and Toughness. ACS Applied Materials & Interfaces", **11** (2019) 35343–35353. https://doi.org/10.1021/acsami.9b12935.

[50] Q. Chen, H. Chen, L. Zhu, & J. Zheng, "Fundamentals of double network hydrogels", Journal of Materials Chemistry B, **3** (2015) 3654–3676. https://doi.org/10.1039/C5TB00123D.

[51] J. P. Gong, Y. Katsuyama, T. Kurokawa, & Y. Osada, "Double-Network Hydrogels with Extremely High Mechanical Strength", Advanced Materials, **15** (2003) 1155–1158. https://doi.org/10.1002/adma.200304907.

[52] J. P. Gong, "Why are double network hydrogels so tough? ", Soft Matter, **6** (2010) 2583–2590. https://doi.org/10.1039/B924290B.

[53] E. Ducrot, Y. Chen, M. Bulters, R. P. Sijbesma, & C. Creton, "Toughening Elastomers with Sacrificial Bonds and Watching Them Break", Science, **344** (2014) 186–189. https://doi.org/10.1126/science.1248494.

[54] Y. Li, L. Yang, Y. Zeng, Y. Wu, Y. Wei, & L. Tao, "Self-Healing Hydrogel with a Double Dynamic Network Comprising Imine and Borate Ester Linkages", Chemistry of Materials, **31** (2019) 5576–5583. https://doi.org/10.1021/acs.chemmater.9b01301.

[55] S. Li, N. Chen, X. Li, Y. Li, Z. Xie, Z. Ma, J. Zhao, X. Hou, & X. Yuan, "Bioinspired Double-Dynamic-Bond Crosslinked Bioadhesive Enables Post-Wound Closure Care", Advanced Functional Materials, **30** (2020) 2000130. https://doi.org/10.1002/adfm.202000130.

[56] F. Zhuge, J. Brassinne, C.-A. Fustin, E. van Ruymbeke, & J.-F. Gohy, "Synthesis and Rheology of Bulk Metallo-Supramolecular Polymers from Telechelic Entangled Precursors", Macromolecules, **50** (2017) 5165–5175. https://doi.org/10.1021/acs.macromol.7b00646.

[57] A. Winter & U. S. Schubert, "Synthesis and characterization of metallo-supramolecular polymers", Chemical Society Reviews, **45** (2016) 5311–5357. https://doi.org/10.1039/C6CS00182C.

[58] F. Snijkers & D. Vlassopoulos, "Cone-partitioned-plate geometry for the ARES rheometer with temperature control", Journal of Rheology, **55** (2011) 1167–1186. https://doi.org/10.1122/1.3625559.

[59] S. Costanzo, Q. Huang, G. Ianniruberto, G. Marrucci, O. Hassager, & D. Vlassopoulos, "Shear and Extensional Rheology of Polystyrene Melts and Solutions with the Same Number of Entanglements", Macromolecules, **49** (2016) 3925–3935. https://doi.org/10.1021/acs.macromol.6b00409.

[60] S. Costanzo, G. Ianniruberto, G. Marrucci, & D. Vlassopoulos, "Measuring and assessing first and second normal stress differences of polymeric fluids with a modular cone-partitioned plate geometry", Rheologica Acta, **57** (2018) 363–376. https://doi.org/10.1007/s00397-018-1080-1.

[61] F. Zhuge, "Synthesis and dynamics of metallo-supramolecular polymeric assemblies", PhD thesis, UCL - Université Catholique de Louvain, 2018.

[62] F. Snijkers, K. Ratkanthwar, D. Vlassopoulos, & N. Hadjichristidis, "Viscoelasticity, Nonlinear Shear Start-up, and Relaxation of Entangled Star Polymers", Macromolecules, **46** (2013) 5702–5713. https://doi.org/10.1021/ma400662b.

[63] G. Petekidis, D. Vlassopoulos, & P. N. Pusey, "Yielding and flow of sheared colloidal glasses", Journal of Physics: Condensed Matter, **16** (2004) S3955–S3963. https://doi.org/10.1088/0953-8984/16/38/013.

[64] S.-J. Xie & K. S. Schweizer, "Consequences of Delayed Chain Retraction on the Rheology and Stretch Dynamics of Entangled Polymer Liquids under Continuous Nonlinear Shear Deformation", Macromolecules, **51** (2018) 4185–4200. https://doi.org/10.1021/acs.macromol.8b00671.

[65] F. Snijkers, D. Vlassopoulos, G. Ianniruberto, G. Marrucci, H. Lee, J. Yang, & T. Chang, "Double Stress Overshoot in Start-Up of Simple Shear Flow of Entangled Comb Polymers", ACS Macro Letters, **2** (2013) 601–604. https://doi.org/10.1021/mz400236z.

[66] K. Osaki, T. Inoue, & T. Isomura, "Stress overshoot of polymer solutions at high rates of shear; Polystyrene with bimodal molecular weight distribution", Journal of Polymer Science Part B: Polymer Physics, **38** (2000) 2043–2050. https://doi.org/10.1002/1099-0488(20000801)38:15<2043::AID-POLB90>3.0.CO;2-F.

[67] K. Osaki, T. Inoue, & T. Isomura, "Stress overshoot of polymer solutions at high rates of shear", Journal of Polymer Science Part B: Polymer Physics, **38** (2000) 1917–1925. https://doi.org/10.1002/1099-0488(20000715)38:14<1917::AID-POLB100>3.0.CO;2-6.

[68] S. Schneider, G. Brehm, C.-J. Prenzel, W. Jäger, M. I. Silva, H. D. Burrows, & S. T. Formosinho, "Vibrational Spectra, Normal Coordinate Analysis and Excited-State Lifetimes for a Series of Polypyridylruthenium(II) Complexes", Journal of Raman Spectroscopy, **27** (1996) 163–175. https://doi.org/10.1002/(SICI)1097-4555(199602)27:2<163::AID-JRS942>3.0.CO;2-N.

[69] B. G. G. Lohmeijer, "Playing LEGO with macromolecules : connecting polymer chains using terpyridine metal complexes", PhD thesis, Technische Universiteit Eindhoven, 2004. https://doi.org/10.6100/IR581839.

SUPPLEMENTARY MATERIAL

Nonlinear shear rheology of single and double metal-ligand dynamic networks

Christina Pyromali[1,2*], Yanzhao Li[3], Flanco Zhuge[3], Charles-André Fustin[3], Evelyne van Ruymbeke[3] and Dimitris Vlassopoulos[1,2]

[1]Institute of Electronic Structure & Laser, FORTH, Heraklion 71110, Crete, Greece

[2] Department of Materials Science and Technology, University of Crete, Heraklion 71003, Crete, Greece

[3]Bio-and Soft Matter, Institute of Condensed Matter and Nanosciences, Université Catholique de Louvain, Croix du Sud 1, B-1348 Louvain-la-Neuve B-1348, Belgium

Contents:

Metal-Ligand binding constant:

Table S1 lists the theoretical binding constants for forming mono- and bis-terpyridine complexes for the three transition metal ions studied. Although these parameters constitute a good indication of thermodynamic and kinetic equilibrium, they correspond to different conditions, i.e., ion-terpyridine association and dissociation in water at 25^{o}C.

Table S1. Binding constants for formation mono-complexes, K_1 and bis-complexes, K_2, along with the association and disassociation constants. Taken from [22, 61].

	K_1 [M^{-1}]	K_2 [M^{-1}]	$\beta=K_1 \cdot K_2$
Zn(II)	10^6	$10^{5.2}$	$10^{11.2}$
Cu (II)	10^{12}	10^6	10^{18}
Co (II)	$10^{8.4}$	$10^{9.9}$	$10^{18.3}$

Rheometry:

The temperature equilibration of the sample before linear and nonlinear shear measurements was followed by Dynamic Time Sweep tests with constant strain amplitude. In addition, Dynamic Frequency Sweeps were conducted between different step-rate tests in order to ensure reproducible steady-state conditions and exclude flow-induced, changes in the linear rheological response.

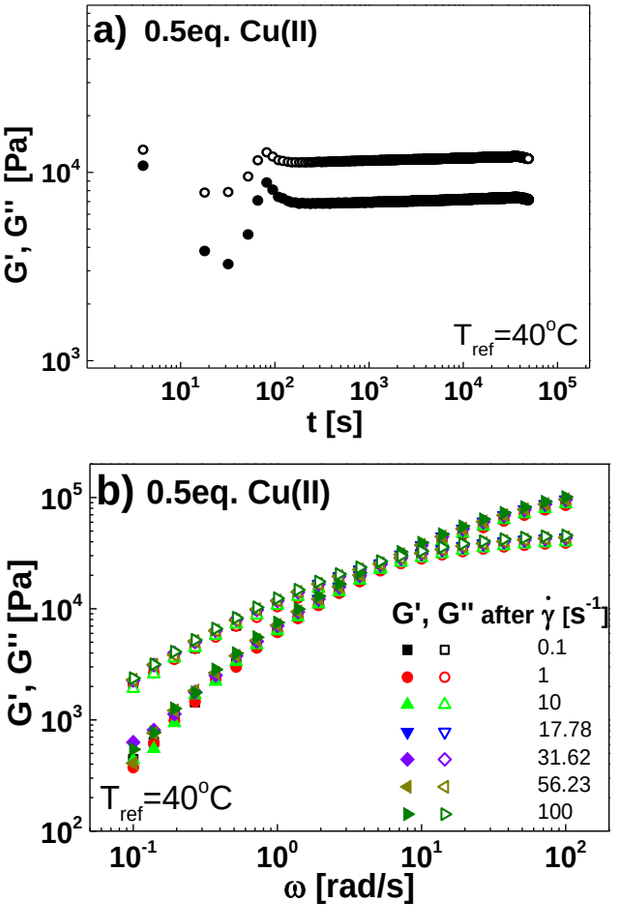

Figure S1. (a) Dynamic time sweeps for temperature equilibration of Star250k+0.5 eq. Cu (II). (b) Dynamic frequency sweeps after step-rate tests (rates indicated in legend). The storage modules is represented with filled symbols and the loss modulus with unfilled symbols.

Differential Scanning Calorimetry:

Differential Scanning Calorimetry (DSC) traces are reported in Figure S2 for Cu-type networks with increasing ion content. The glass transition temperature (T_g) remains reasonably unchanged (± 1°C) for the three samples. On the other hand, the second weak transition is related to ligand exchange mechanism that appears to slow-down as the crosslinking density of the dynamic bond increase.

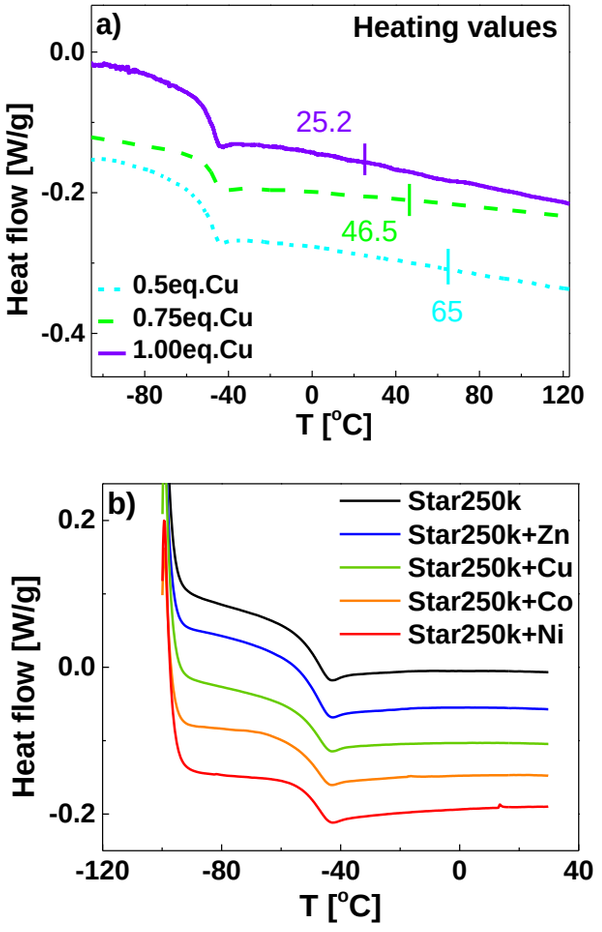

Figure S2. Top: DSC second heating curves of Star250k networks with different amounts 0.5eq., 0.75eq. and 1.0eq. of Cu (II) with rate 10K/min (traces are shifted vertically for clarity). Glass transition (-60°C) and the secondary transition are evaluated as the midpoint using TRIOS software. Bottom: Respective

DSC curves of Star250k networks with 0.5 eq. of different metal ions, as indicated in the legend. The reference sample is also included.

Table S2. Glass transition temperatures for networks based on Star250k with 0.5eq. and different metal ions (the reference sample is also included).

Sample	T_g [°C]
Star250k	-52
Star250k+Zn	-51
Star250k+Cu	-51
Star250k+Co	-51
Star250k+Ni	-51

Data analysis of transient measurements of single and double dynamics networks.

The ratio of the steady-state to complex viscosity is plotted for all single transient networks in Figure S3. The comparison is made at the same rate and frequency, respectively. This ratio is higher than unity which corresponds to the extent of failure of the Cox-Merz rule. The latter is common feature (not necessarily universal) of associative polymers.

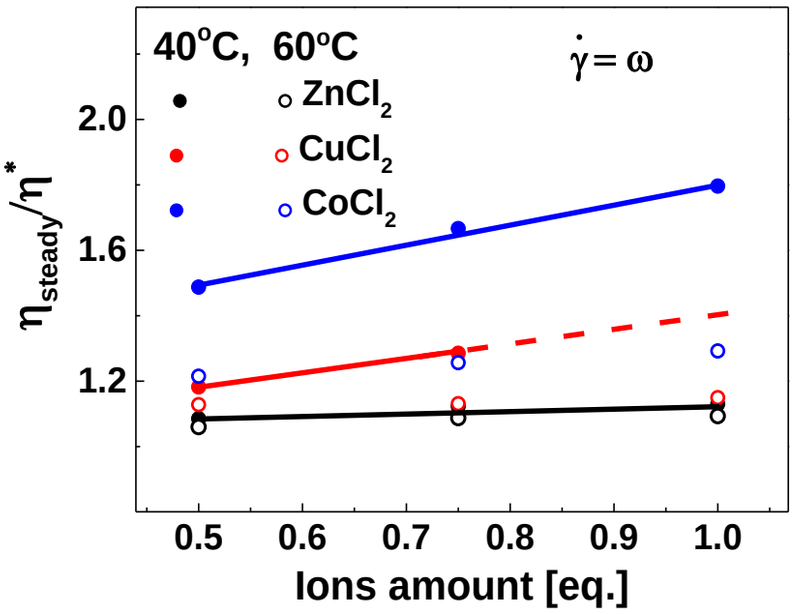

Figure S3. Viscosity ratio as a function of ion content for different ion-ligand strengths and temperatures at $\omega = \dot{\gamma} = 10s^{-1}$. Dashed line represents extraplotation of 1.00eq. Cu data at 40°C (measurement was not possible due to macroscopic failure of the sample).

The steady-state shear viscosities are normalized with complex viscosity, $\eta_0 = G_N^0 \ \tau_d$, where G_N^0 is the experimental determined plateau modulus, extracted from the minimum of $tan\delta$, and τ_d is the experimentally determined longest relaxation time from the low-frequency moduli crossover at the same reference temperature. These data are plotted against the Weissenberg number ($Wi = \dot{\gamma}\tau_d$).

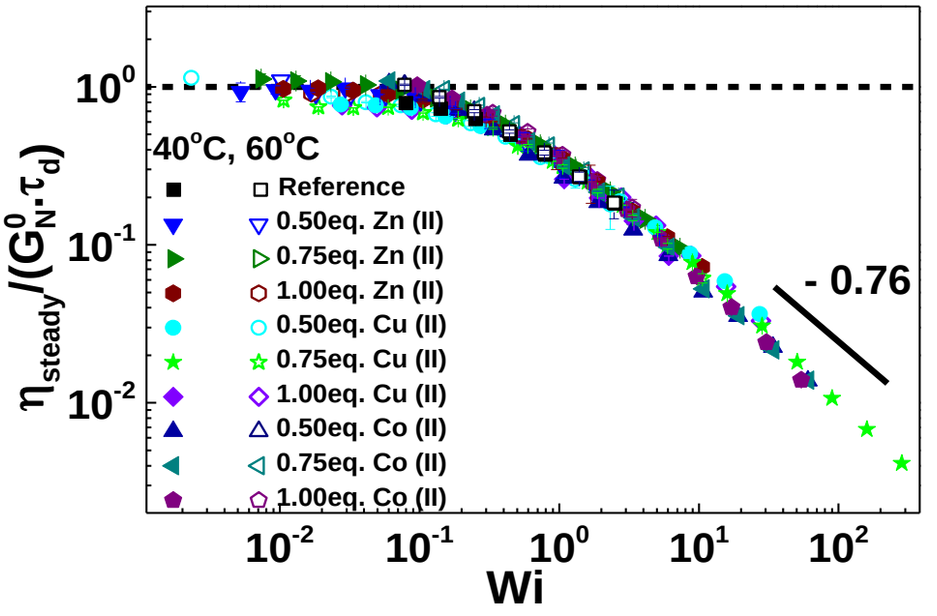

Figure S4. Normalized steady-state shear viscosities as a function of the Weissenberg number for the reference sample and the single ion systems as a temperature of 40°C and 60°C (resulting in a thinning slope of -0.76). Error bars are at the size of the symbols.

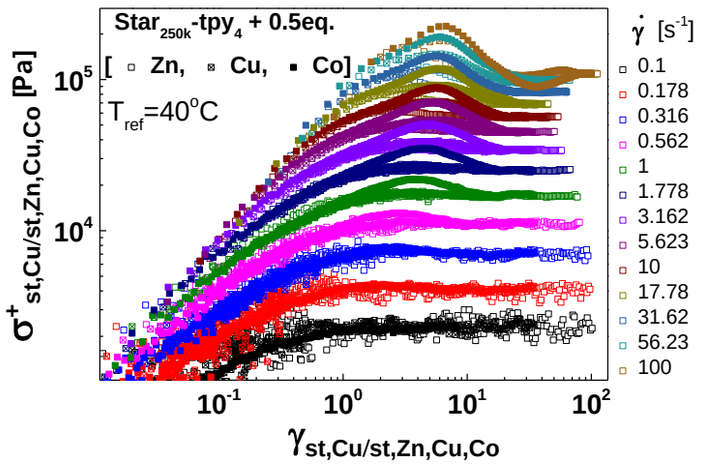

Figure S5. Shifted shear stress growth function versus shifted strain (with respect to a reference value, see text) of single dynamics networks with different association types at 40°C. Three selected rates are shown in Figure 6 of the main text.

In order to compare the broadness of the peak for Cu-type dynamic networks with increasing ion content, the shear stress growth function is normalized with the overshoot values. The broadness ($\Delta t/t_{max}$) is estimated as the width at half-height of the peak.

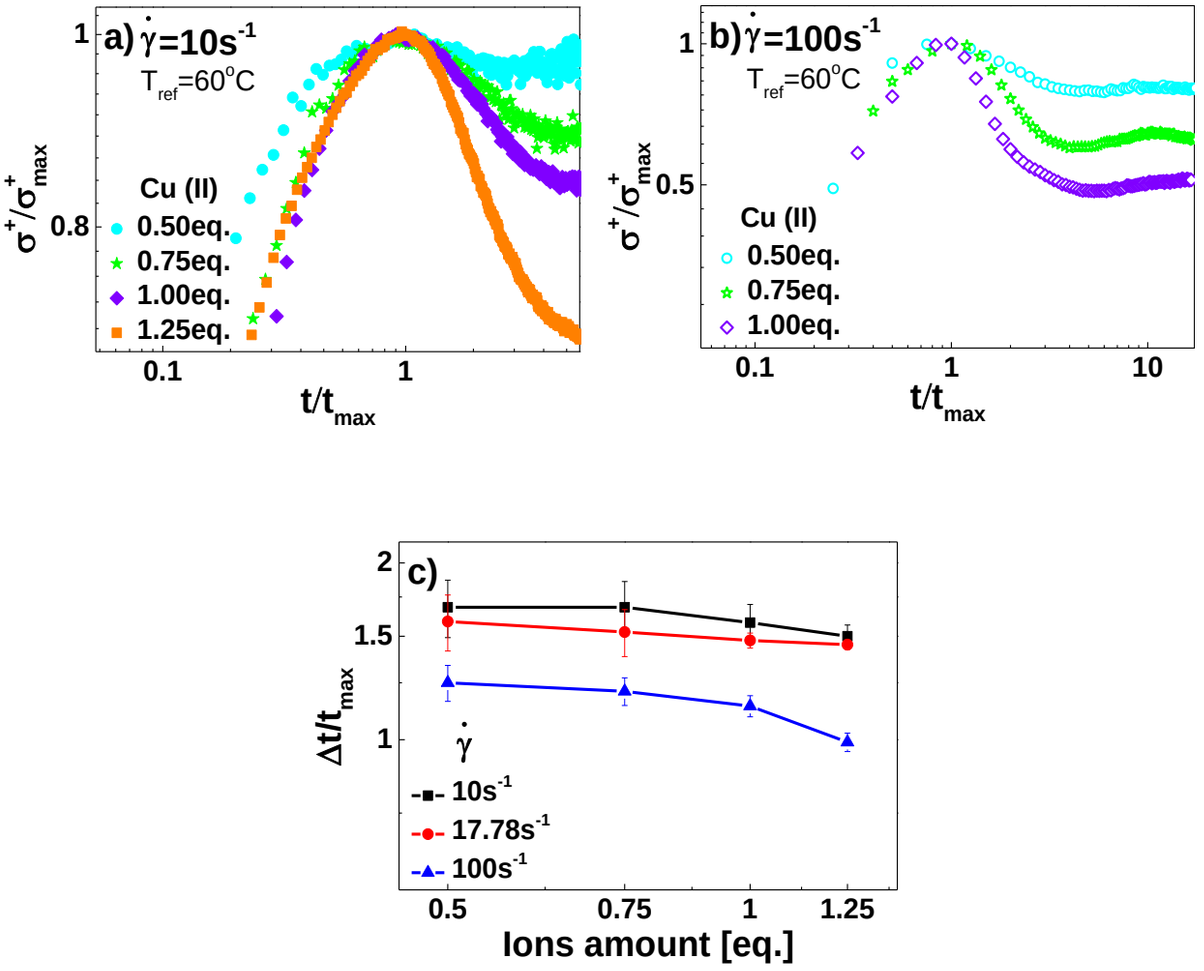

Figure S6. (a) Normalized shear stress growth function for Cu-type transient networks with different ion content at 10s^{-1}. (b) Similar data at 100s^{-1}. (c) Width at half height of overshoot for Cu-type transient networks 40°C with different ion content at rates 10s^{-1}, 17.78 s^{-1} and 100s^{-1}.

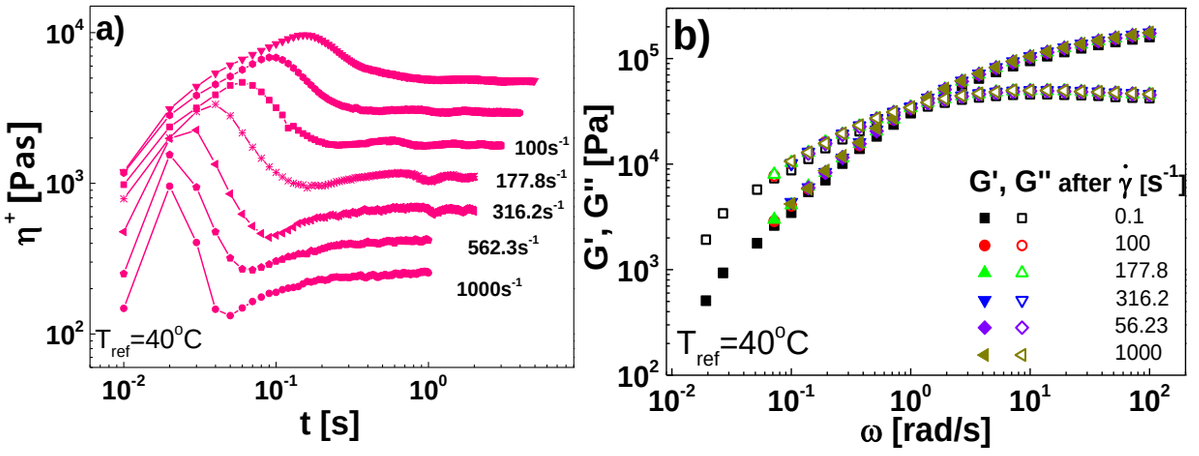

Figure S7. Transient (a) and dynamic measurements (b) for supramolecular double dynamics networks with 1.0eq. [Zn + Cu] at 40°C.

The failure of the Cox-Merz rule for double dynamics networks is weaker than the corresponding single network components (Figure 3 of main text). Double dynamics appear to eliminate breakage of the longer and stronger metal-ligand complexes due to the (sacrificial) weak component.

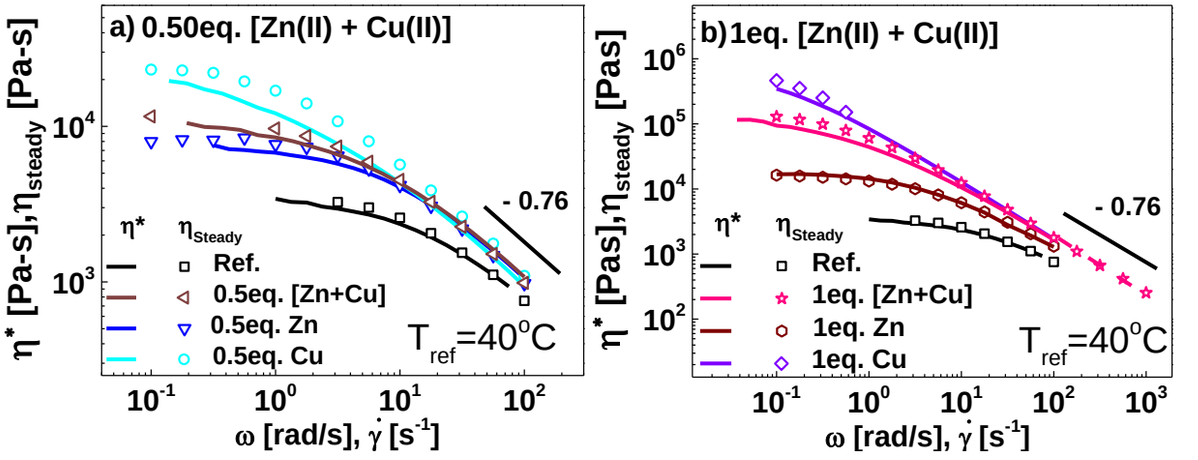

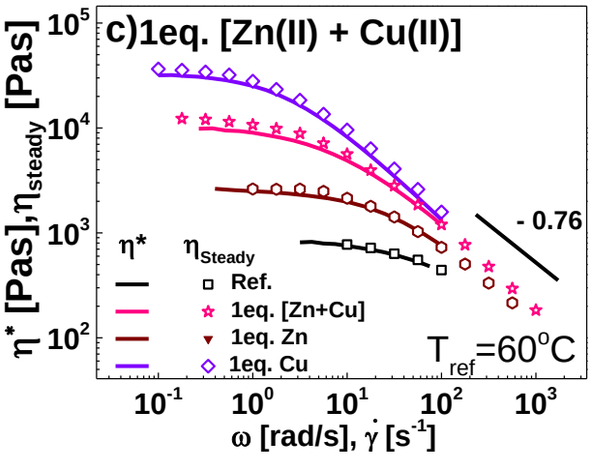

Figure S8. Cox-Merz rule for supramolecular double dynamics networks with (a) 0.5eq. [Zn + Cu] at 40°C, (b) 1eq. [Zn + Cu] at 40°C, and (c) 1eq. [Zn + Cu] at 60°C, along with the corresponding single network components.

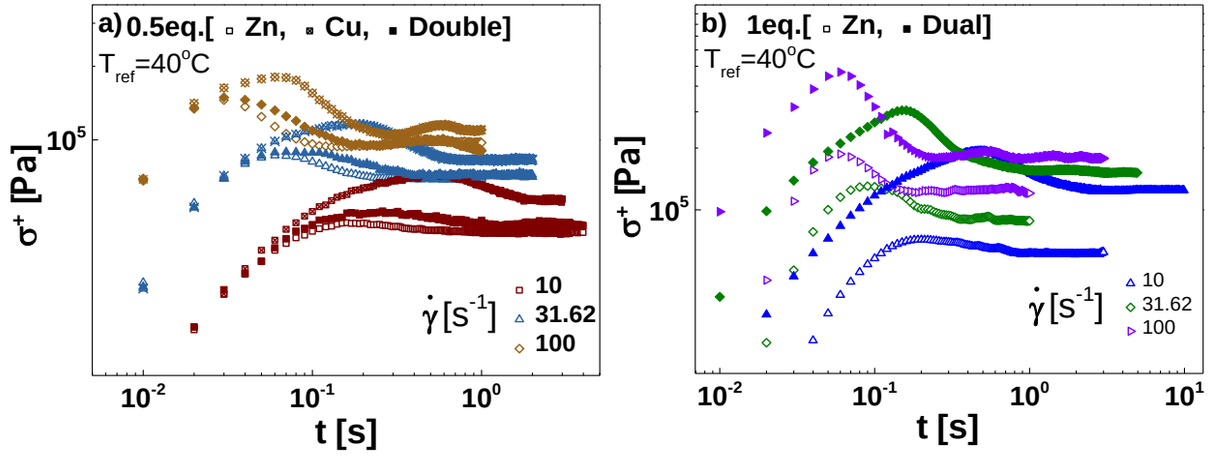

Figure S9. Shear stress growth functions of single and double dynamics networks based on Zn-ions and Cu-ions, at 40°C and different rates (indicated in the legends), for different ion amounts: (a) 0.5eq. and (b) 1.0eq.

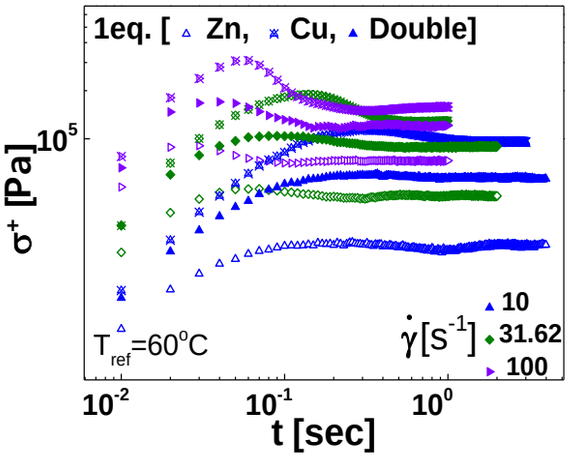

Figure S10. Shear stress growth functions of single and double dynamics networks based on Zn-ions and Cu-ions at 60°C and different rates.

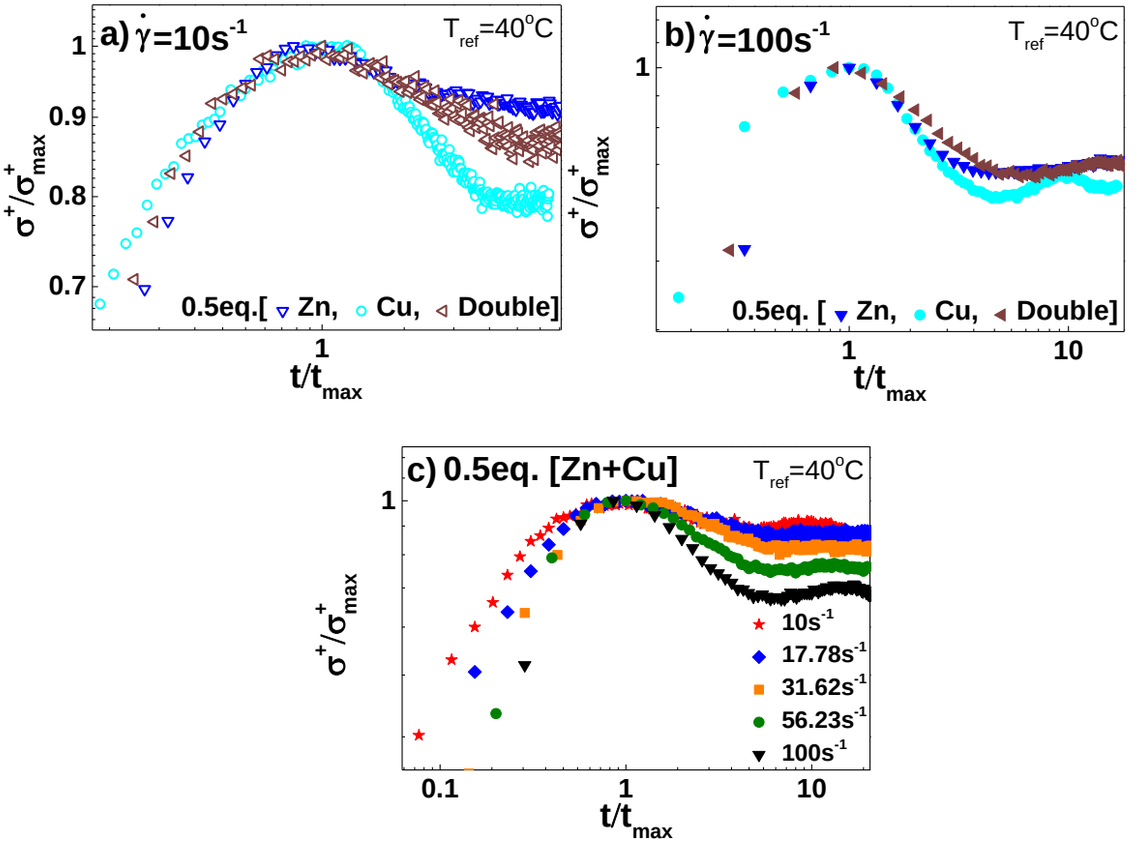

Figure S11. (a) Normalized shear stress growth function for single and respective double dynamics networks with 0.50eq. [Zn (II) + Cu(II)] at $10s^{-1}$. (b) Similar data at $100s^{-1}$. (c) Evolution of peak broadness with shear rate for double dynamics network with 0.50eq. [Zn (II) + Cu(II)] at 40°C.

πάντα ῥεῖ

Journal of Rheology ACCEPTED MANUSCRIPT

This is the author's peer reviewed, accepted manuscript. However, the online version of record will be different from this version once it has been copyedited and typeset.
PLEASE CITE THIS ARTICLE AS DOI: 10.1122/8.0000429

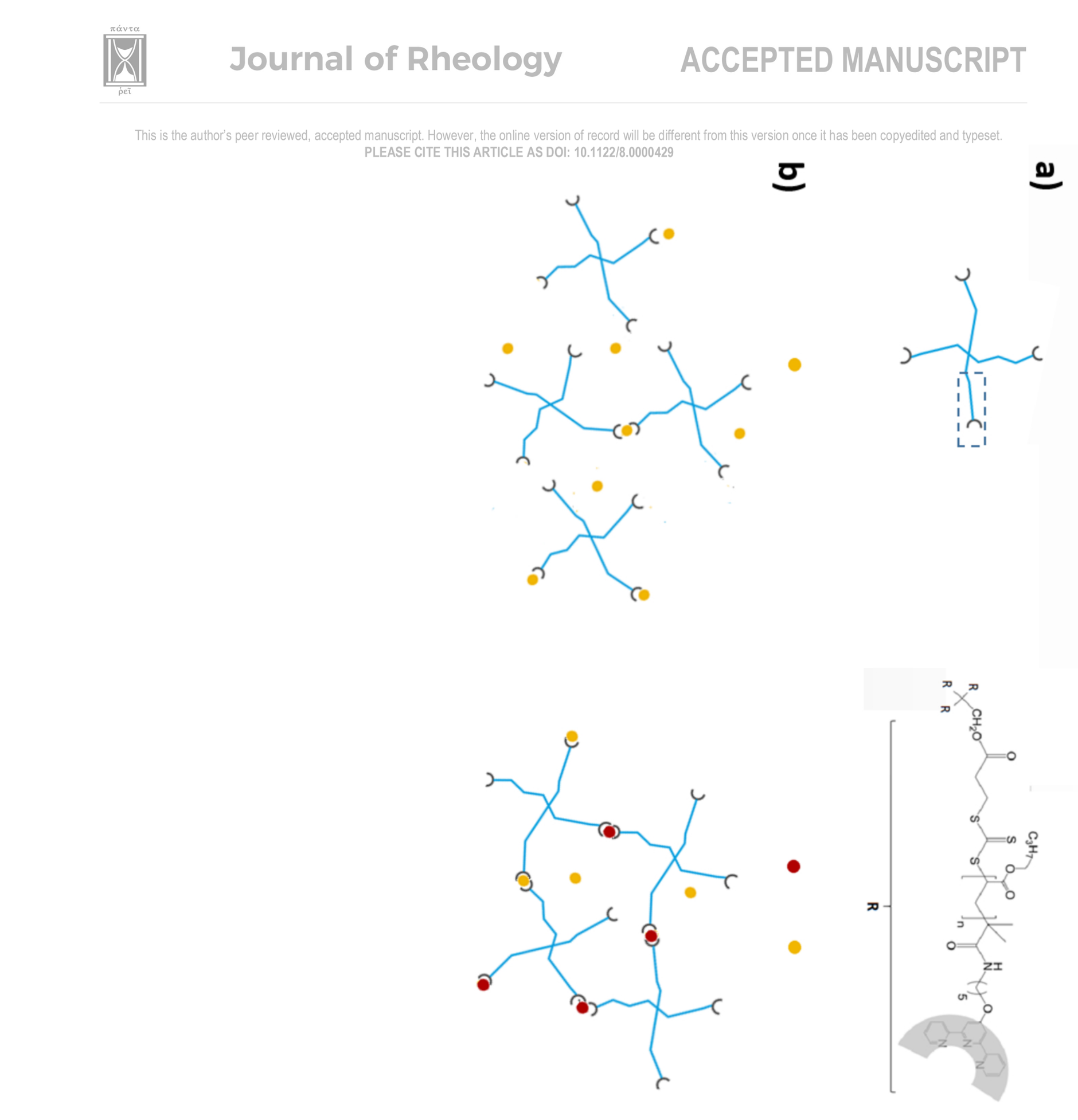

Journal of Rheology

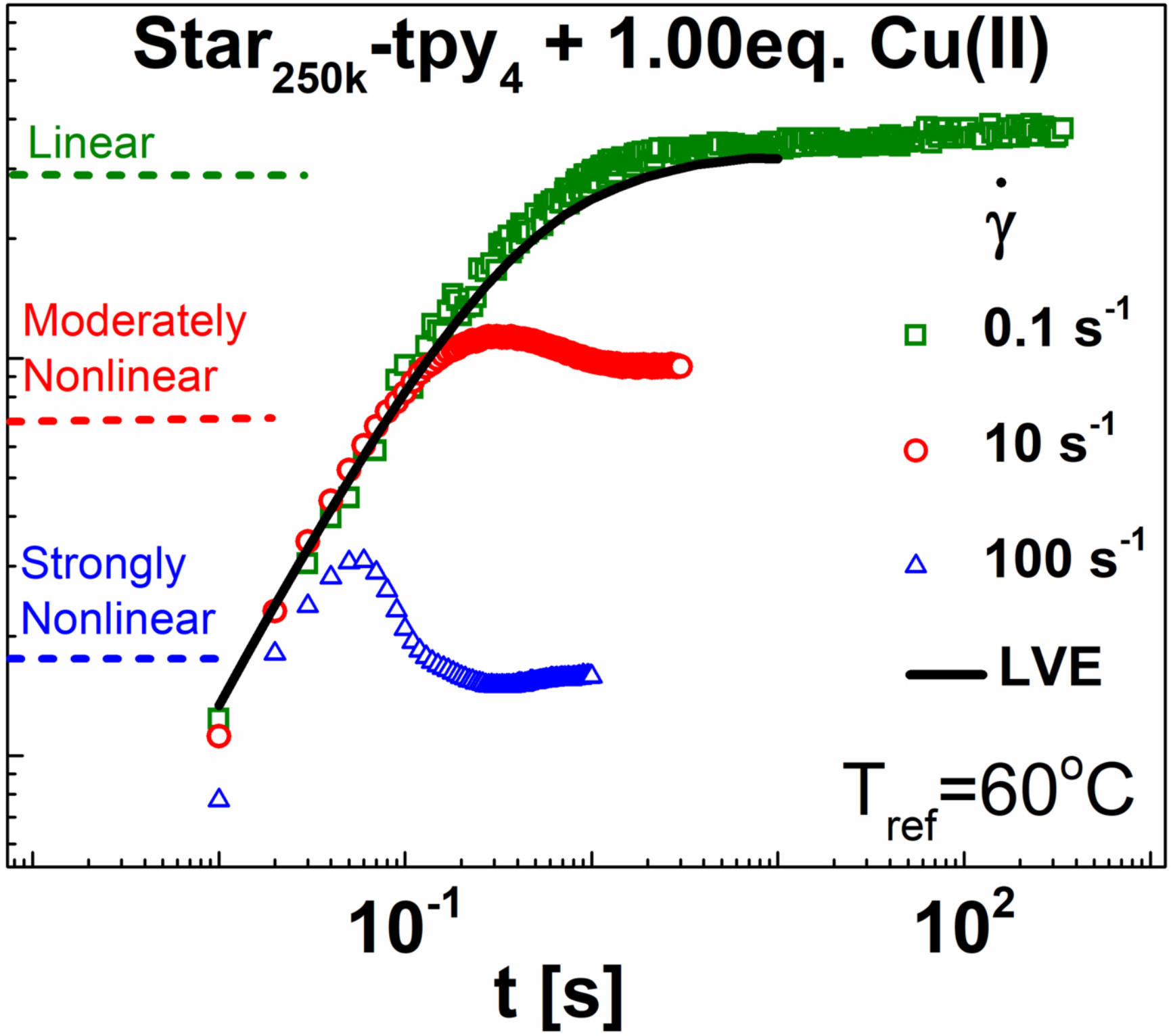

Journal of Rheology

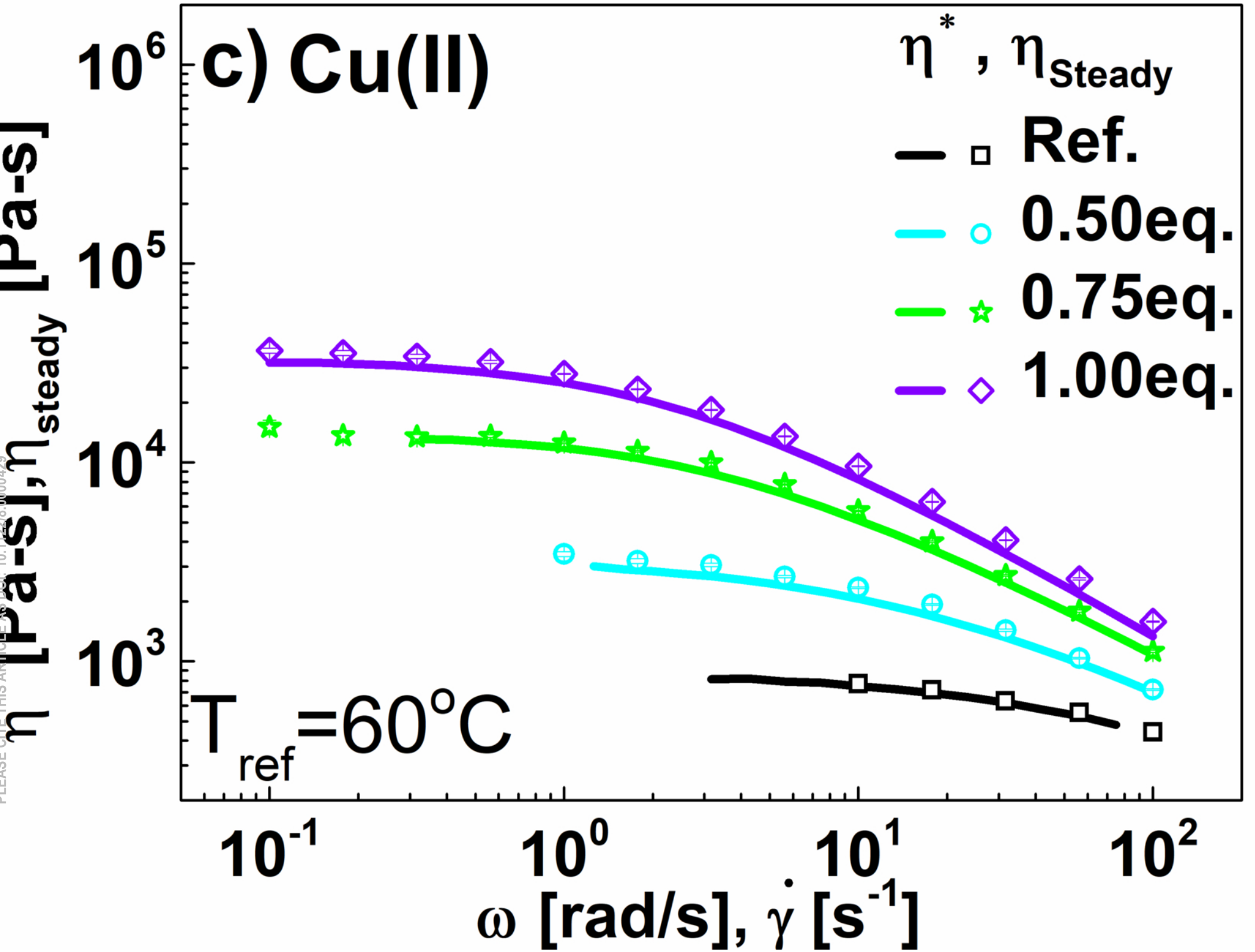

Journal of Rheology

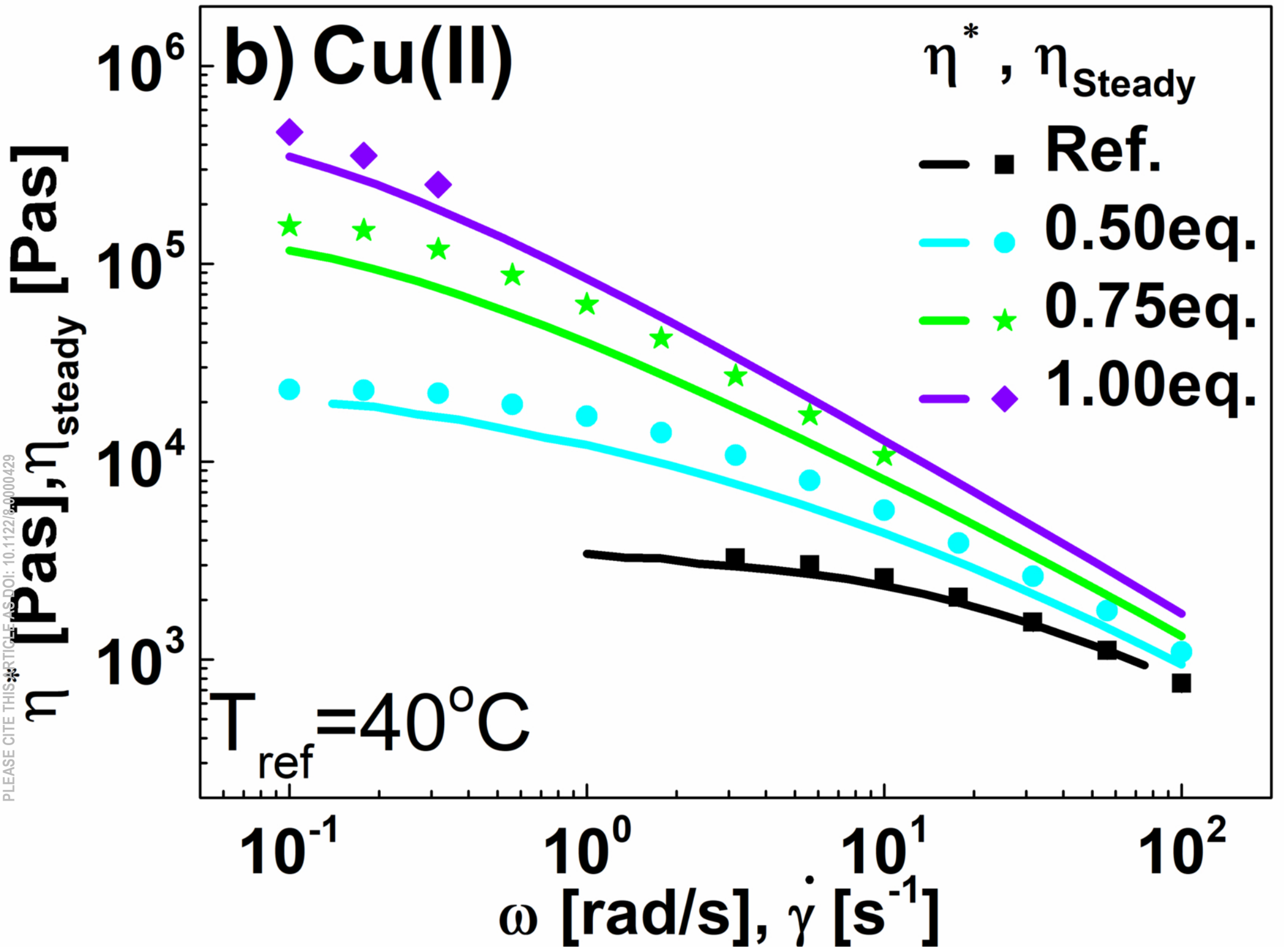

Journal of Rheology

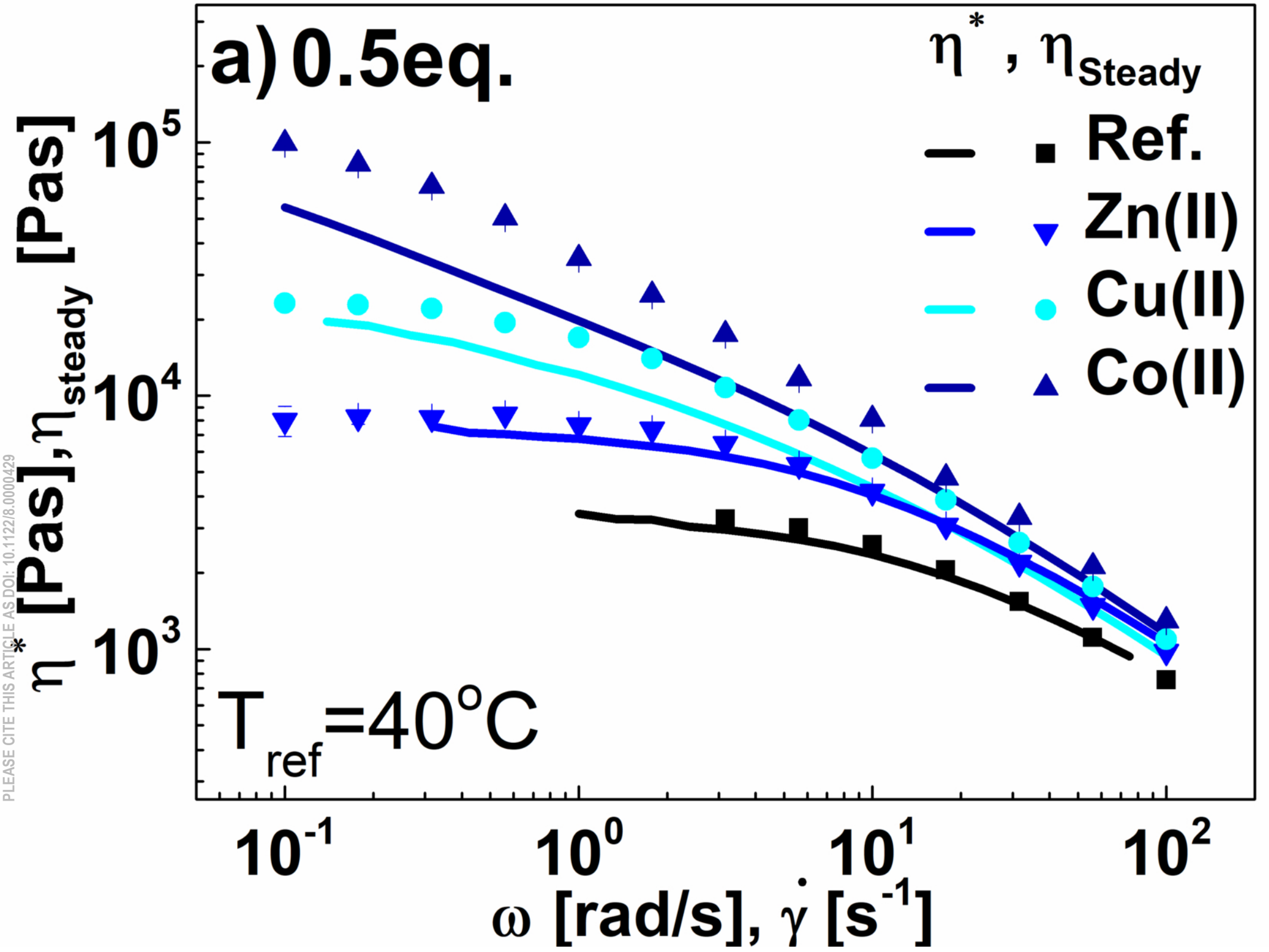

Journal of Rheology

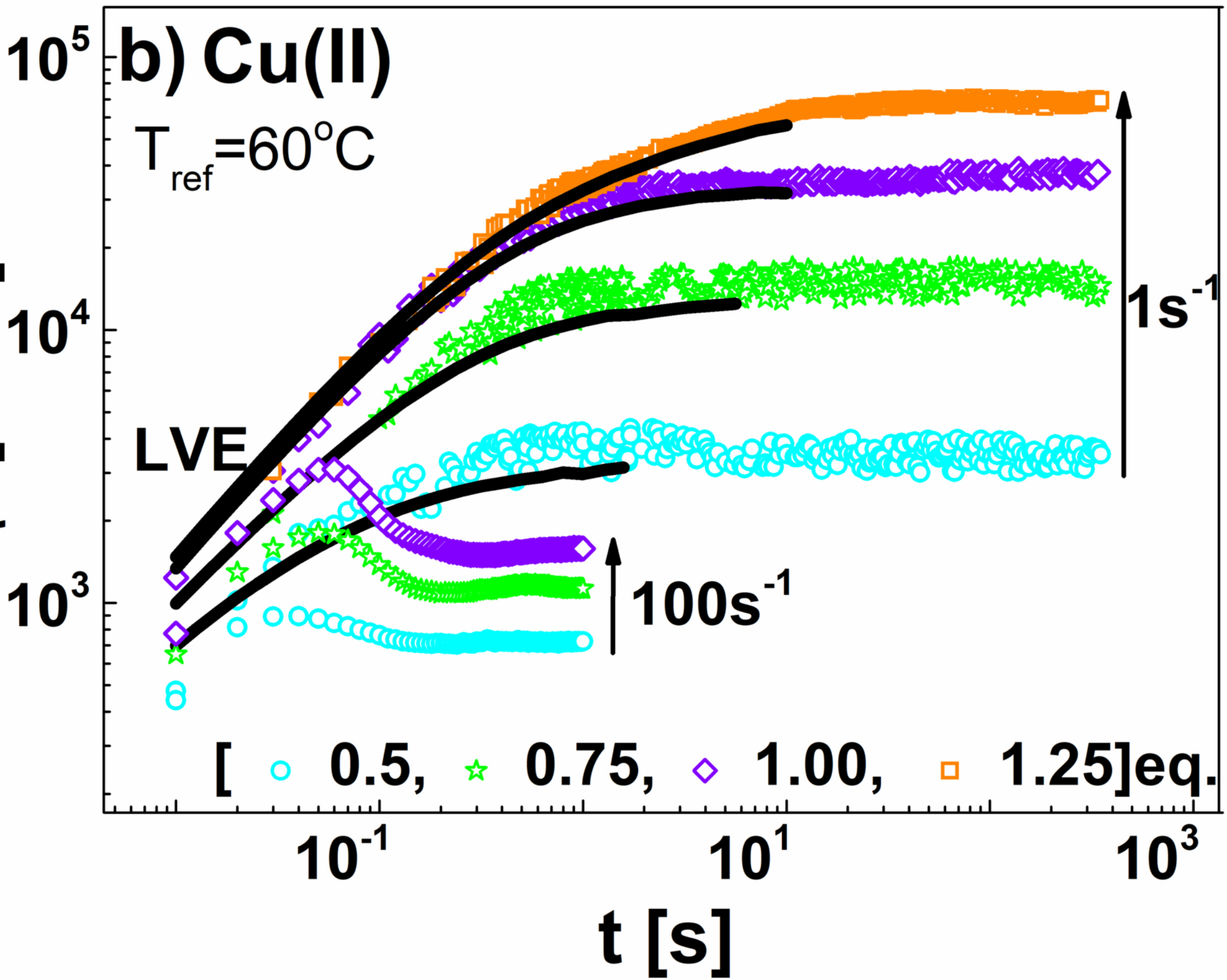

Journal of Rheology

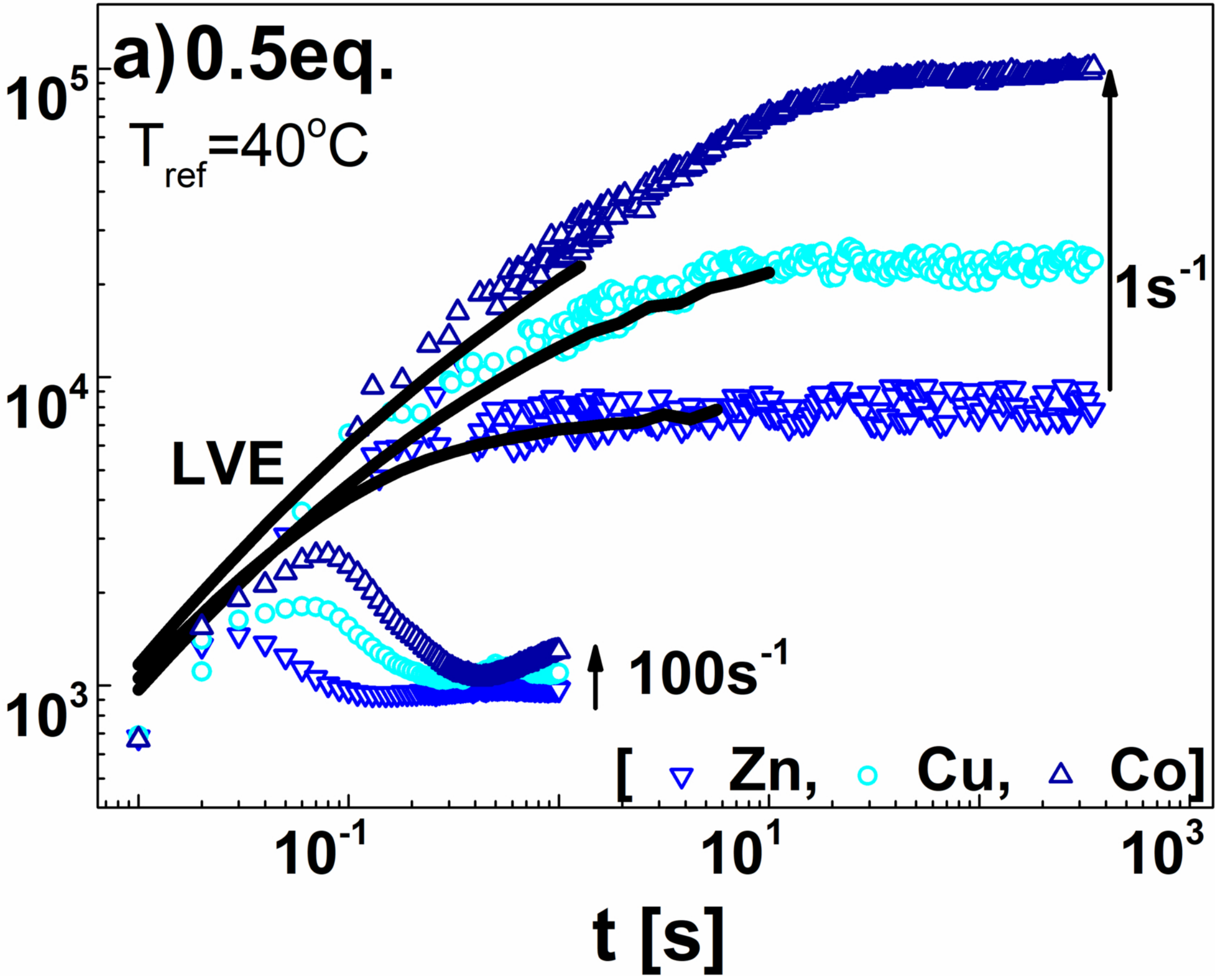

Journal of Rheology

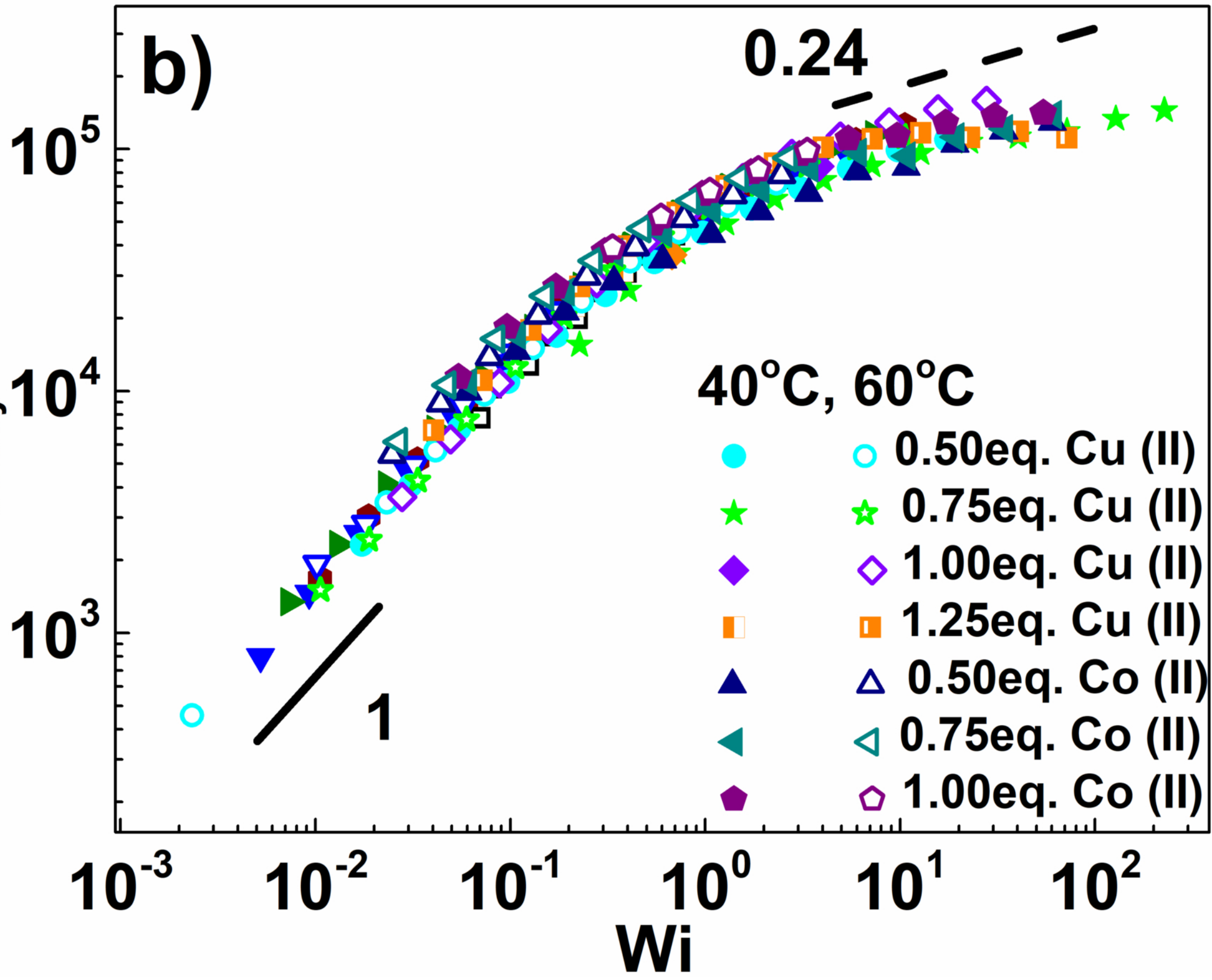

Journal of Rheology

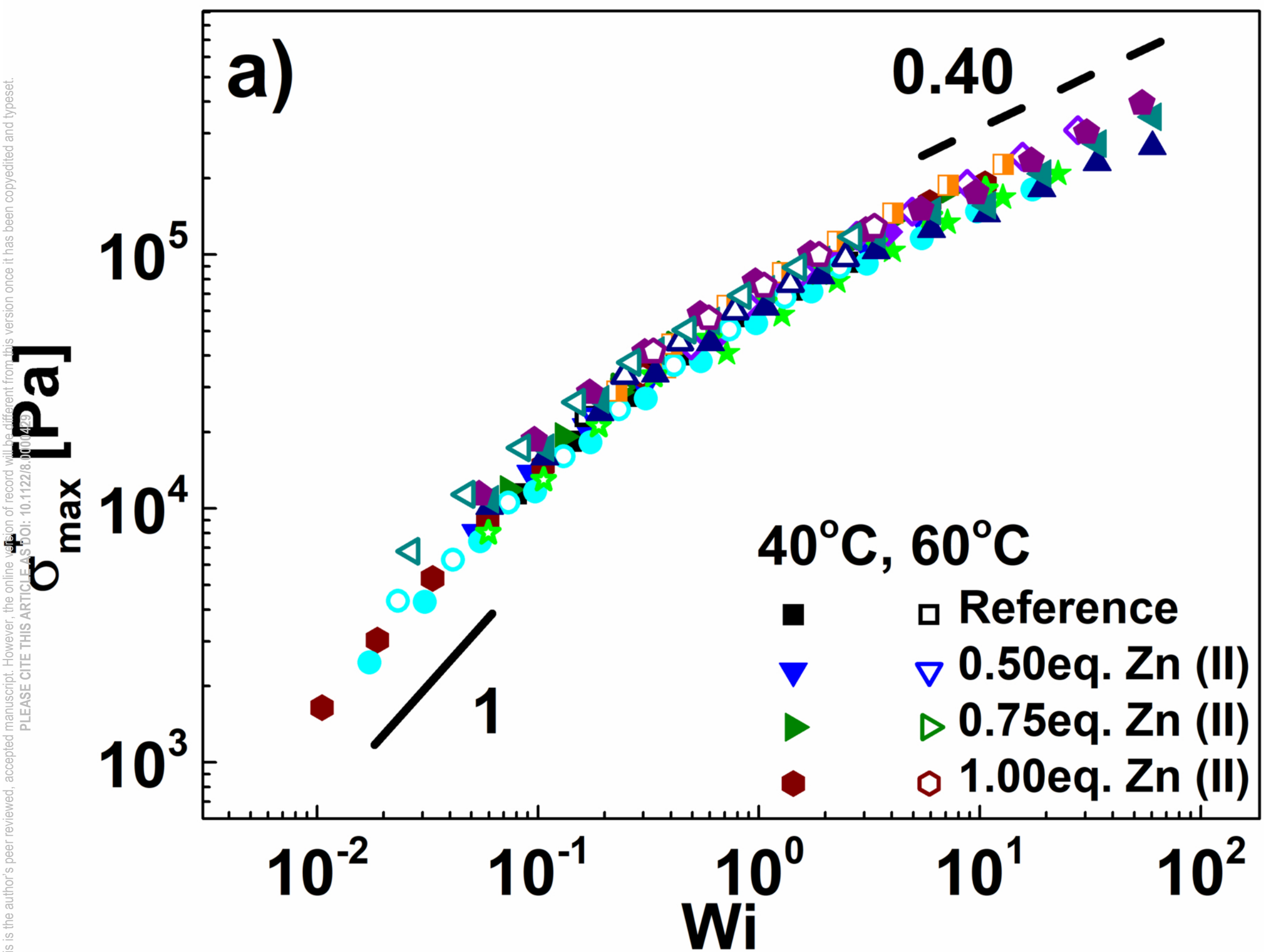

Journal of Rheology

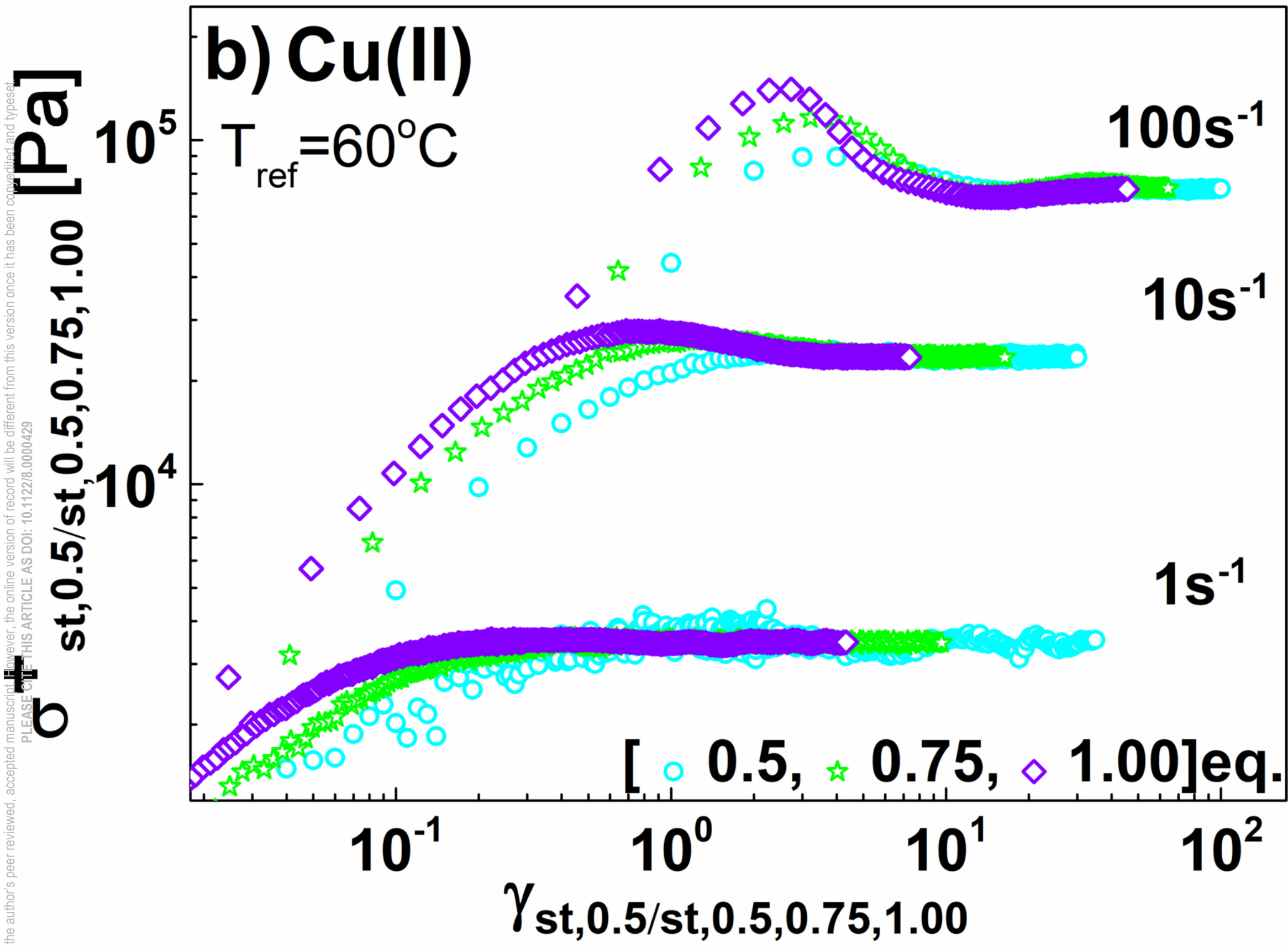

Journal of Rheology

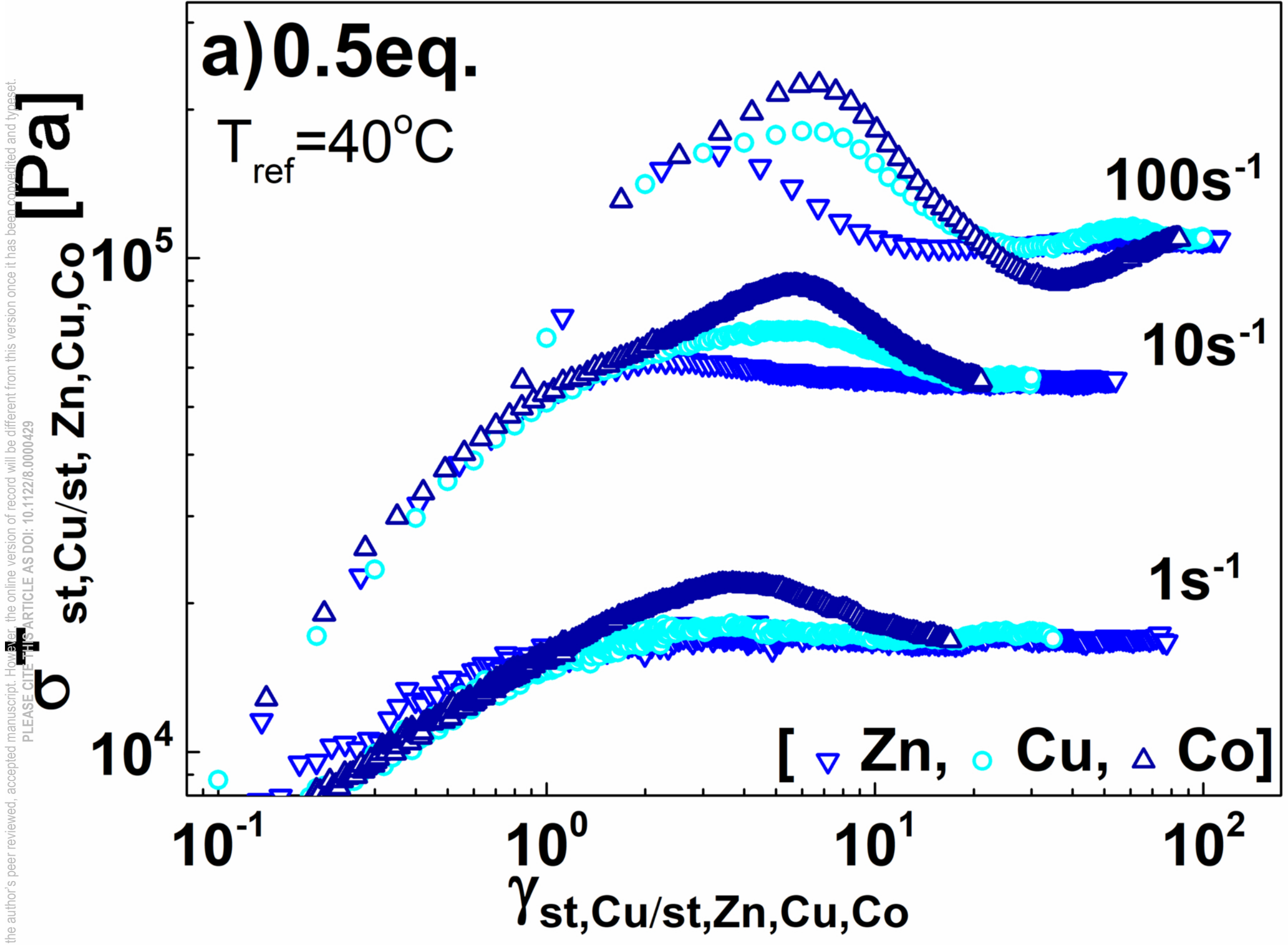

Journal of Rheology

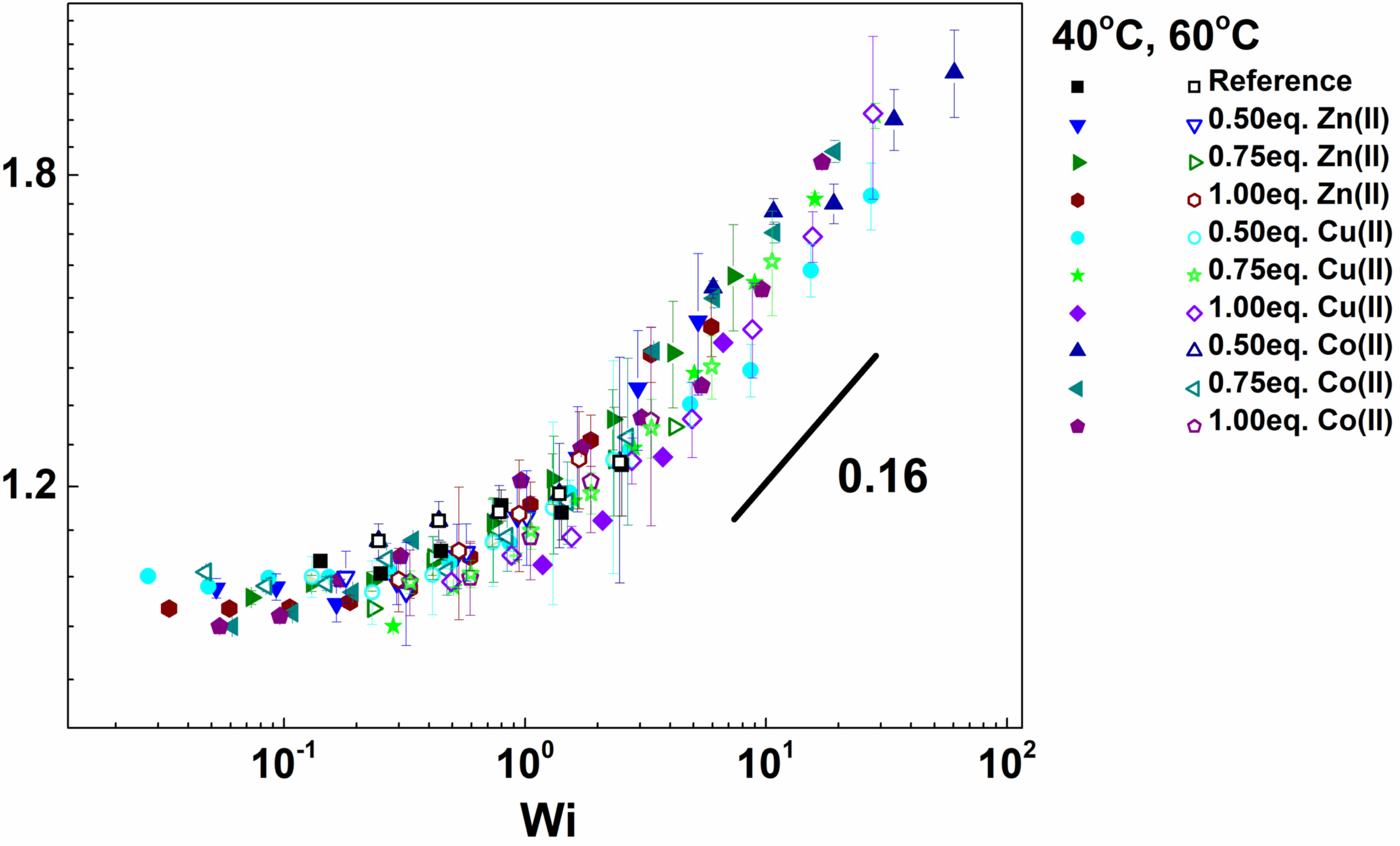

Journal of Rheology

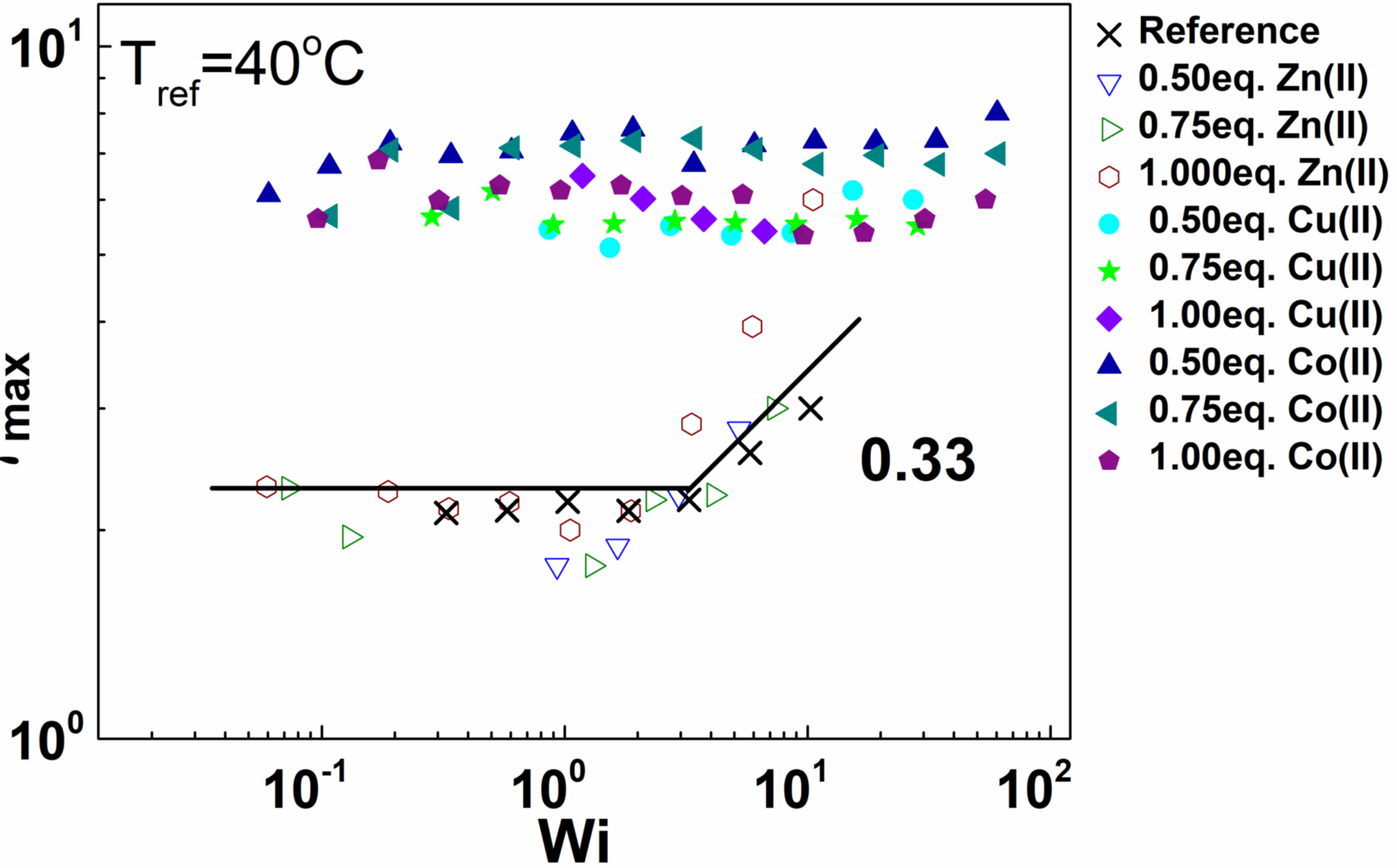

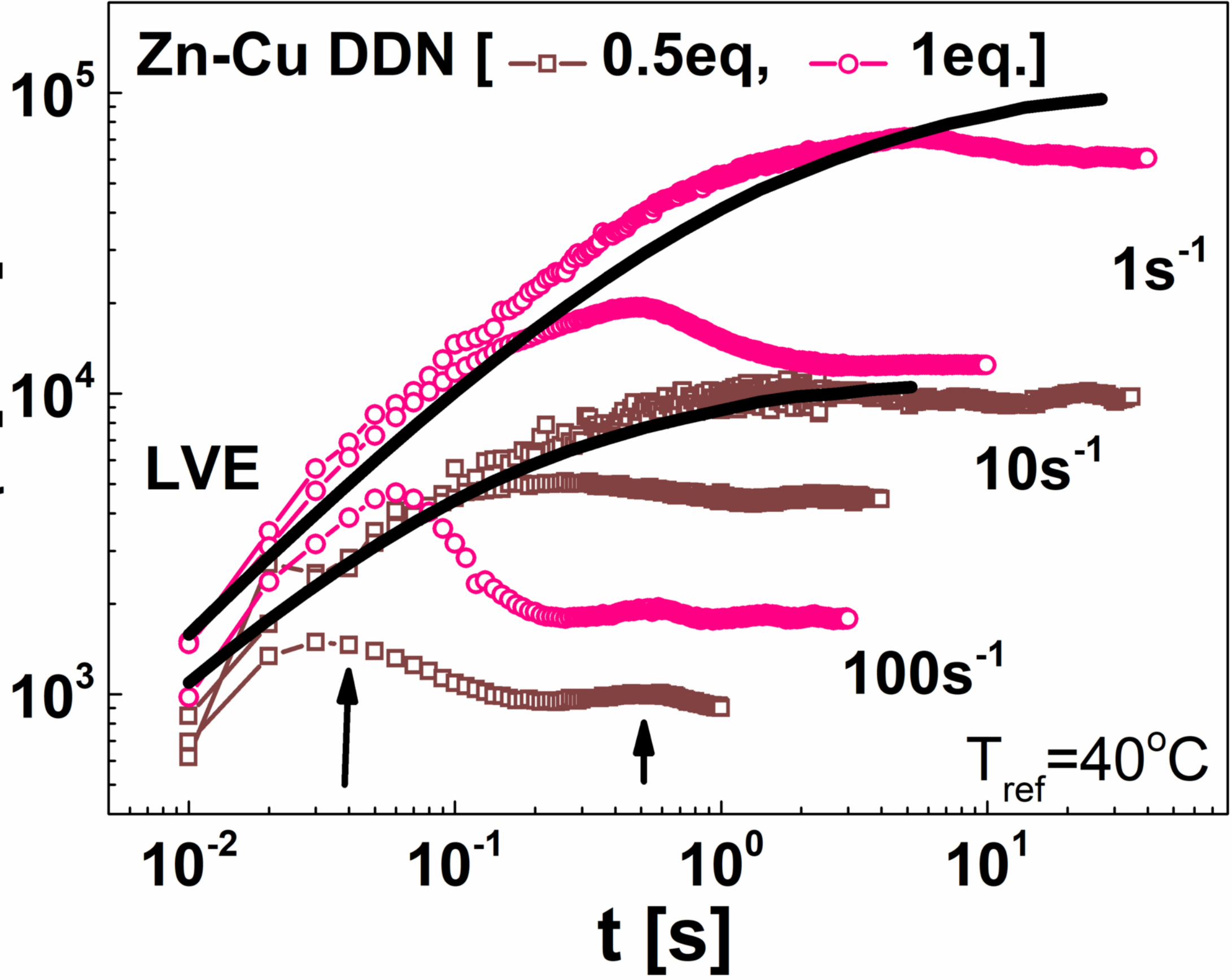

Journal of Rheology

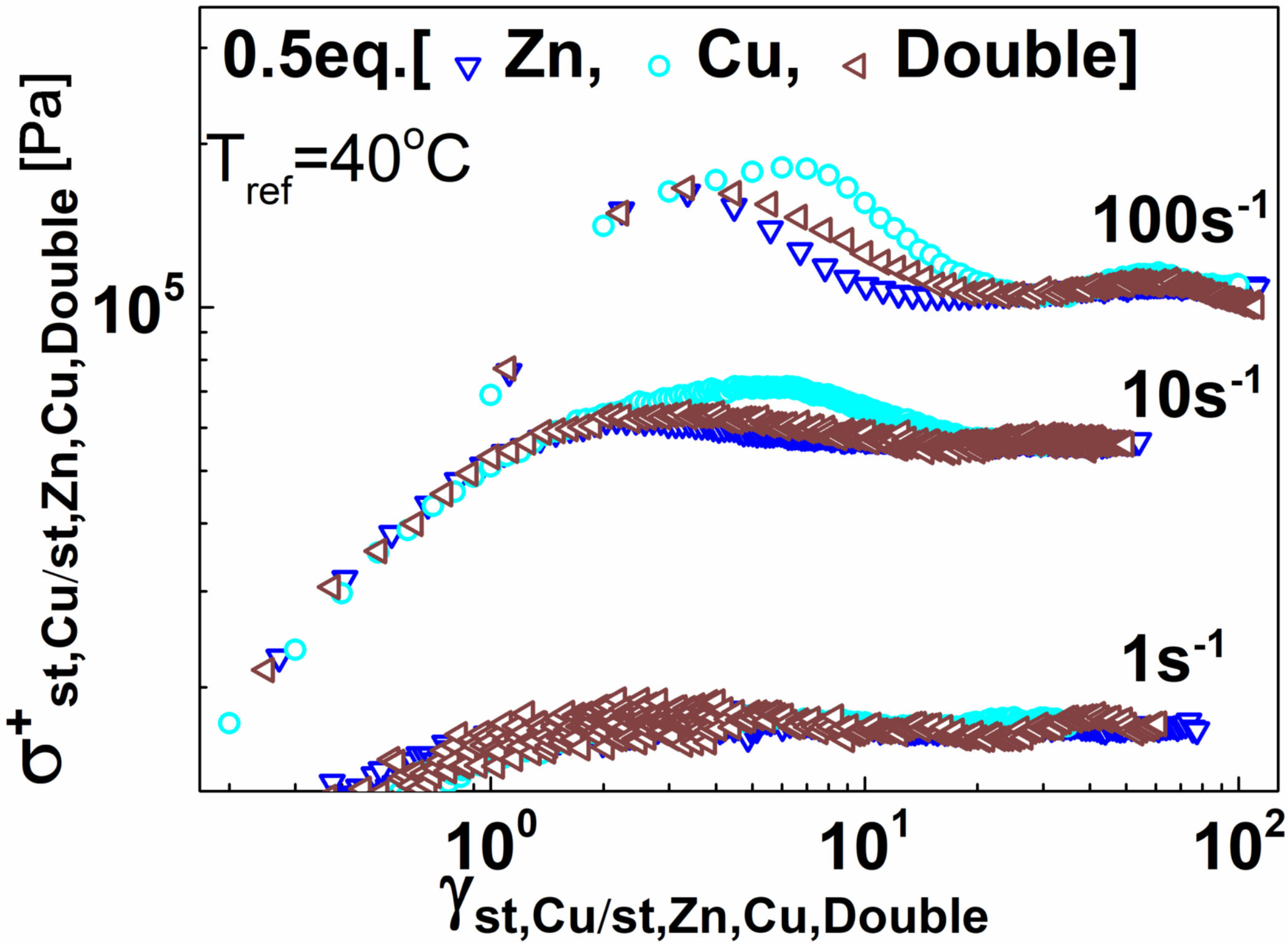

Journal of Rheology

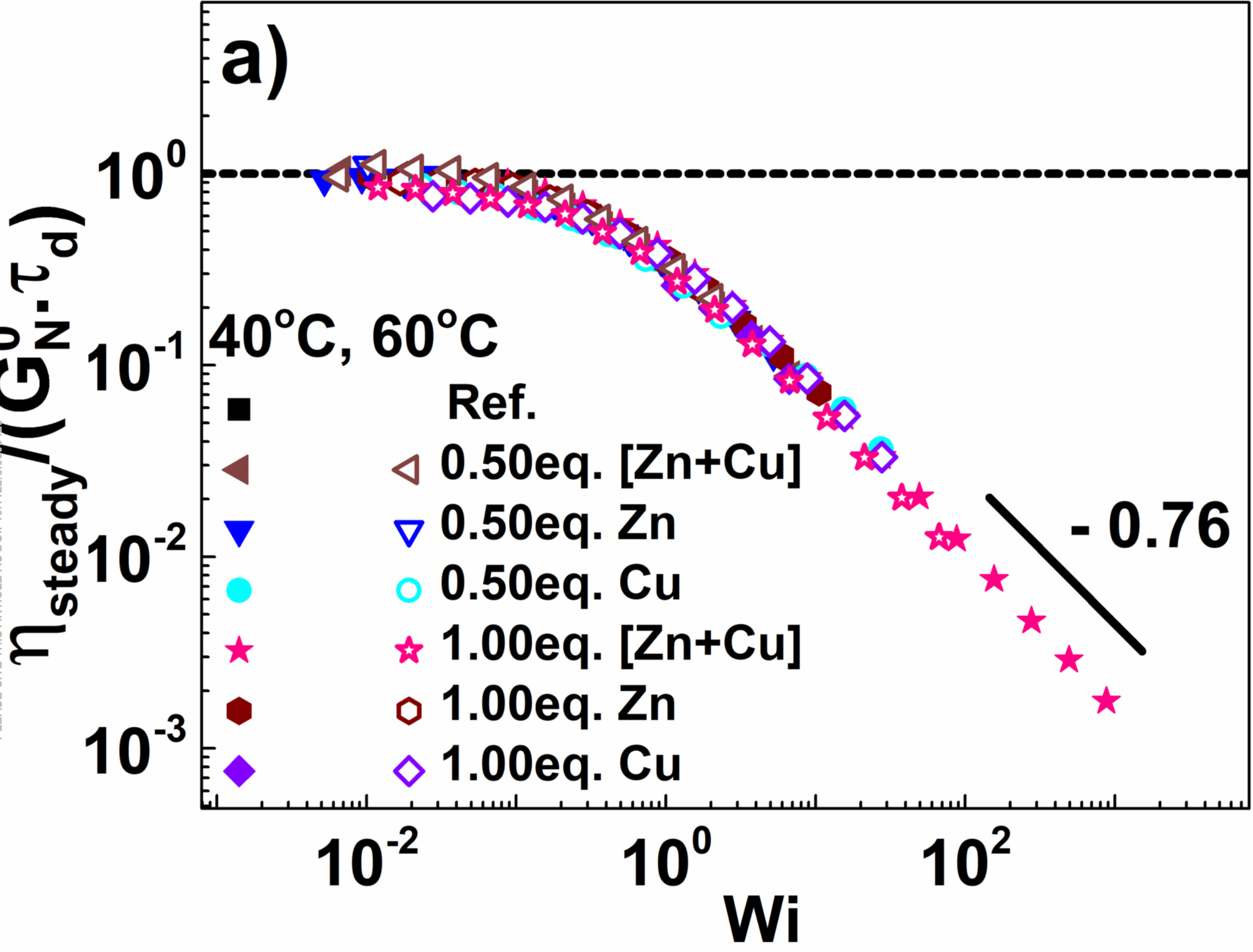

Journal of Rheology